

1
2
3
4
5
6
7
8
9
10
11
12
13
14
15
16
17
18
19
20
21
22

Deploying dengue-suppressing *Wolbachia*:

robust models predict slow but effective spatial spread in *Aedes aegypti*

Michael Turelli^{1*}, Nicholas H. Barton²

¹ Department of Evolution and Ecology, University of California, Davis,
California, United States of America

² Institute of Science and Technology, Am Campus 1, A-3400 Klosterneuburg,
Austria

* Corresponding author

email: mturelli@ucdavis.edu (MT)

Running Head: Deploying dengue-suppressing *Wolbachia*

Keywords: population transformation; population replacement; bistable dynamics; disease suppression; Zika; biocontrol; wave theory; mutualistic endosymbiont

11 December 2016

1 **Abstract**

2 A novel strategy for controlling the spread of arboviral diseases such as dengue, Zika and
3 chikungunya is to transform mosquito populations with virus-suppressing *Wolbachia*. In general,
4 *Wolbachia* transinfected into mosquitoes induce fitness costs through lower viability or
5 fecundity. These maternally inherited bacteria also produce a frequency-dependent advantage for
6 infected females by inducing cytoplasmic incompatibility (CI), which kills the embryos produced
7 by uninfected females mated to infected males. These competing effects, a frequency-dependent
8 advantage and frequency-independent costs, produce bistable *Wolbachia* frequency dynamics.
9 Above a threshold frequency, denoted \hat{p} , CI drives fitness-decreasing *Wolbachia* transinfections
10 through local populations; but below \hat{p} , infection frequencies tend to decline to zero. If \hat{p} is not
11 too high, CI also drives spatial spread once infections become established over sufficiently large
12 areas. We illustrate how simple models provide testable predictions concerning the spatial and
13 temporal dynamics of *Wolbachia* introductions, focusing on rate of spatial spread, the shape of
14 spreading waves, and the conditions for initiating spread from local introductions. First, we
15 describe data from *Aedes aegypti* populations near Cairns, Australia that demonstrate long-
16 distance dispersal and provide an approximate lower bound on \hat{p} for *wMel* in northeastern
17 Australia. Second, we use approximations for \hat{p} and dispersal distances to predict the outcome
18 of 2013 releases of *wMel*-infected *Aedes aegypti* in Cairns, Australia, using idealized diffusion
19 models of temporal and spatial dynamics. Third, we consider the robustness of diffusion-based
20 predictions to incorporating two important features of *wMel-Aedes aegypti* biology that may be
21 inconsistent with the diffusion approximations, namely fast local dynamics induced by complete
22 CI (*i.e.*, all embryos produced from incompatible crosses die) and long-tailed, non-Gaussian
23 dispersal. With complete CI, long-tailed dispersal changes wave-width predictions only slightly;
24 but it can significantly reduce wave speed relative to the diffusion prediction; it also allows
25 smaller local introductions to initiate spatial spread. Finally, we apply our analyses to produce
26 operational guidelines for efficient transformation of vector populations over large areas. We
27 demonstrate that even very slow spatial spread, on the order of 10-20 m/month (as predicted),

- 1 can produce area-wide population transformation within a few years following initial releases
- 2 covering about 20-30% of the target area.
- 3

1 **Introduction**

2 *Wolbachia* are maternally inherited endosymbionts, pervasive among arthropods (Weinert et al.
3 2015) and best known for reproductive manipulation (Werren et al. 2008). Their most widely
4 documented reproductive manipulation is cytoplasmic incompatibility (CI) (Hoffmann and
5 Turelli 1997; Hamm et al. 2014), which kills embryos produced by *Wolbachia*-uninfected
6 females mated to infected males. *Wolbachia*-infected females are compatible with both infected
7 and uninfected males and generally produce only infected progeny. CI gives infected females a
8 reproductive advantage that increases with the infection frequency. Consequently, CI-inducing
9 *Wolbachia* can spread within and among populations, at least once they become sufficiently
10 common that the CI-induced advantage overcomes any frequency-independent disadvantages
11 (Caspari and Watson 1959; Turelli and Hoffmann 1991; Turelli 2010; Barton and Turelli 2011).
12 Because *Wolbachia* are maternally transmitted, selection favors variants that increase the fitness
13 of infected females (Turelli 1994; Haywood and Turelli 2009). This fosters the evolution of
14 adaptive phenotypes including pathogen protection, whereby *Wolbachia*-infected individuals are
15 protected from some pathogens, including viruses (Hedges et al. 2008; Teixeira et al. 2008).
16 Pathogen protection is not universal (Osborne et al. 2009), and studies of both transient somatic
17 *Wolbachia* transinfections (Dodson et al. 2014) and stable transinfections (Martinez et al. 2014)
18 suggest that *Wolbachia* can occasionally enhance susceptibility to pathogens. However, virus
19 protection seems to be a common property of both natural and introduced *Wolbachia* infections
20 (Martinez et al. 2014).

21 This anti-pathogen effect has revitalized efforts to use *Wolbachia* for disease control, an
22 idea first proposed in the 1960s (Laven 1967; McGraw & O'Neill 2013). The disease-vector
23 mosquito *Aedes aegypti* has been transinfected with two *Wolbachia* strains from *Drosophila*
24 *melanogaster* (*w*MelPop, McMeniman et al. 2009; and *w*Mel, Walker et al. 2011). Two isolated
25 natural Australian *Ae. aegypti* populations have been transformed with *w*Mel to suppress dengue
26 virus transmission (Hoffmann et al. 2011), and these populations have remained stably

1 transformed for more than four years (Hoffmann et al. 2014; S. L. O’Neill, pers. comm.). The
2 dengue-suppressing phenotype of *wMel*-transinfected *Ae. aegypti*, first demonstrated in
3 laboratory colonies (Walker et al. 2011), has been maintained, and possibly enhanced, after two
4 years in nature (Frentiu et al. 2014). Recently, *wMel* has also been shown to block the spread of
5 the Zika virus by *Ae. aegypti* (Dutra et al. 2016). *Anopheles stephensi* was also transinfected with
6 *Wolbachia*, making them less able to transmit the malaria-causing parasite (Bian et al. 2013).
7 *Wolbachia* transinfections are now being deployed for disease control in at least five countries
8 (Australia, Vietnam, Indonesia, Brazil and Colombia, see the “Eliminate Dengue” website:
9 <http://www.eliminatedengue.com/program>), with many more releases planned. We present
10 simple approximation-based predictions to aid and understand the deployment of these
11 transinfections.

12 Our mathematical analyses rest on bistable frequency dynamics for *Wolbachia*
13 transinfections. Namely, the frequency-independent costs associated with introduced infections
14 cause frequencies to decline when the infections are rare; but the frequency-dependent advantage
15 associated with CI overcomes these costs when the infections become sufficiently common. As
16 explained below, bistability now seems implausible for naturally occurring *Wolbachia* infections,
17 as explained below (cf. Fenton et al. 2011; Kriesner et al. 2013; Hamm et al. 2014). However,
18 we present several lines of evidence, including new field data, indicating that *wMel*
19 transinfections in *Ae. aegypti* experience bistable dynamics.

20 Turelli and Hoffmann (1991) proposed bistable dynamics to describe the northward spread
21 of *Wolbachia* variant *wRi* through California populations of *D. simulans*. The rationale for
22 bistability was that the frequency-dependent advantage associated with CI seemed to be
23 counteracted at low frequencies by two factors: imperfect maternal transmission, whereby a few
24 percent of the ova produced by infected mothers were uninfected (Hoffmann et al. 1990; Turelli
25 and Hoffmann 1995; Carrington et al. 2011); and reduced fecundity for infected females, with a
26 10-20% fecundity disadvantage observed in the lab (Hoffmann and Turelli 1988, Hoffmann et al.

1 1990; Nigro and Prout 1990) and a smaller, but statistically significant, fecundity disadvantage
2 observed once in nature (Turelli and Hoffmann 1995).

3 The generality of bistable frequency dynamics for natural *Wolbachia* infections was brought
4 into question by two infections found first in Australia that cause little (*wMel* in *D.*
5 *melanogaster*, Hoffmann 1988; Hoffmann et al. 1998) or no (*wAu* in *D. simulans*, Hoffmann et
6 al. 1996) CI or other reproductive manipulation (Hoffmann and Turelli 1997). It was
7 subsequently discovered that these *Wolbachia* nevertheless spread in nature. First noted was a
8 turnover of *Wolbachia* variants among global populations of *D. melanogaster* (Riegler et al.
9 2005; Richardson et al. 2012), even though none of these variants cause appreciable CI when
10 males are more than a few days old (Reynolds and Hoffmann 2002; Harcombe and Hoffmann
11 2004). Similarly, *Wolbachia* variant *wAu*, which does not cause CI in *D. simulans* (Hoffmann et
12 al. 1996), was found spreading to intermediate frequencies through *D. simulans* populations in
13 eastern Australia, despite imperfect maternal transmission (Kriesner et al. 2013). The spread of
14 *wAu* was followed by the spread of *wRi* through these same populations, beginning from three
15 widely separated geographical locations (Kriesner et al. 2013). Although spread of bistable
16 *Wolbachia* could in principle be initiated by chance fluctuations (Jansen et al. 2008), a net fitness
17 advantage that counteracts imperfect transmission seems far more plausible (Hoffmann and
18 Turelli 1997; Fenton et al. 2011; Hamm et al. 2014). The observed rate of spread for *wRi*,
19 approximately 100 km/yr., in both California and eastern Australia, is easy to understand only if
20 long-distance, human-mediated dispersal can establish local infections that spread and coalesce
21 (see Shigesada and Kawasaki 1997, Ch. 5). Such rapid expansion is implausible if local
22 introductions must be sufficiently extensive to exceed initial area and frequency thresholds
23 imposed by bistability (Barton and Turelli 2011). With bistability, spatial spread is likely to be
24 limited by the relatively slow processes of active insect dispersal. As demonstrated below, this
25 indicates that the spread of transinfections with bistable dynamics in *Ae. aegypti* will be orders of
26 magnitude slower than the 100 km/year observed for *wRi* in California and Australia populations
27 of *D. simulans*.

1 A net fitness benefit for natural *Wolbachia* infections helps explain the persistence and
2 spread of *Wolbachia* variants, such as *w*Au and *w*Mel, that do not cause appreciable CI in their
3 native *Drosophila* hosts. A net fitness benefit, so that the relative fitness of infected females, F ,
4 and their maternal transmission rate, $1 - \mu$, satisfy $F(1 - \mu) > 1$, would also help explain the
5 extraordinarily rapid human-mediated spatial spread of *w*Ri in both California and Australia.
6 Mitochondrial data reported in Kriesner et al. (2013) suggest that *w*Ri spread northward in
7 California shortly after it was introduced to southern California, rather than being stalled by a
8 transverse mountain range, as might be expected with bistability (cf. Turelli and Hoffmann
9 1995). Several fitness advantages have been proposed to counteract imperfect transmission and
10 possible fecundity disadvantages, including nutritional effects (Brownlie et al. 2009; Gill et al.
11 2014) and microbe protection (Hedges et al. 2008; Teixeira et al. 2008).

12 These arguments against bistability for natural *Wolbachia* infections may suggest that
13 intrinsic fitness advantages, together with CI, could lead to rapid spread of disease-suppressing
14 *Wolbachia* transinfections in nature from minimal introductions. However, these novel host-
15 *Wolbachia* associations have not been filtered by natural selection. The *w*Mel infection
16 introduced into *Aedes aegypti* reduces fecundity on the order of 20% in laboratory assays, even
17 after persisting in nature for more than two years (Hoffmann et al. 2014). When *w*Mel was
18 successfully introduced into two isolated suburbs near Cairns, Australia, its dynamics implicated
19 fitness costs, on the order of 20%, that slowed establishment (Hoffmann et al. 2011).
20 Furthermore, when a few *w*Mel-infected *Ae. aegypti* were inadvertently introduced to adjacent
21 suburbs, their frequencies rapidly decreased, again suggesting bistability. We present additional
22 empirical support for bistability of *w*Mel-infected *Ae. aegypti*. In particular, persistent
23 immigration over four years from an infected natural population into an uninfected natural
24 population has not led to establishment of *w*Mel.

25 Why does bistability matter? As reviewed in Barton and Turelli (2011), bistability
26 constrains which variants can spread spatially, how fast they spread, how difficult it is to initiate
27 spread, and how easily spread is stopped. Roughly speaking, spatial spread can occur only if the

1 critical frequency, denoted \hat{p} , above which local dynamics predict deterministic increase rather
2 than decrease, is less than a threshold value near $\frac{1}{2}$. As discussed in Turelli (2010), \hat{p} is a
3 threshold frequency below which *Wolbachia* infection frequency tends to decrease and above
4 which it tends to increase. Its value is determined by a balance between the frequency-dependent
5 advantage provided by cytoplasmic incompatibility and frequency-dependent disadvantages
6 associated with possible deleterious *Wolbachia* effects on fecundity, viability and development
7 time. As this threshold is approached, the rate of predicted spatial spread slows to zero, the area
8 in which the variant must be established to initiate spread approaches infinity, and smaller spatial
9 heterogeneities suffice to halt spread. Spatial dynamics depend on details of local frequency
10 dynamics and dispersal that are not well understood. This motivates our exploration of
11 quantitative predictions using relatively simple but robust models that focus on three key
12 biological phenomena, dispersal, deleterious fitness effects and cytoplasmic incompatibility.

13 We seek conditions under which minimal releases of dengue-suppressing *Wolbachia*
14 transinfections achieve area-wide disease control by transforming a significant fraction of the
15 vector population in a relatively short period. We focus on simple models to provide quantitative
16 predictions and guidelines, and test their robustness to long-distance dispersal and discrete
17 spatial distributions. Our simple approximations make testable predictions that may be improved
18 as additional data become available. Many parameters in detailed models will be difficult to
19 estimate and are likely to vary in time and space. Our idealization is motivated by the scarce
20 information concerning the ecology of disease vectors such as *Ae. aegypti*. For instance, the
21 dynamics of introductions must depend on ecological factors such as density regulation
22 (Hancock et al. 2011a,b). However, the ecology of *Ae. aegypti* is so poorly understood that
23 increases in embryo lethality associated with CI might lead to either decreasing or increasing
24 adult numbers (cf. Prout 1980; Walsh et al. 2013; but see Hancock et al. 2016). As in Barton and
25 Turelli (2011), we ignore these complications and emphasize quantitative conclusions that
26 depend on only two key parameters: σ , a measure of average dispersal distance, and \hat{p} , the
27 unstable equilibrium frequency. We illustrate how these two parameters can be estimated from

1 introduced-*Wolbachia* frequency data (producing predictions that can be cross-validated) and
2 explore the robustness of the resulting predictions.

3 Our new analyses build on Barton and Turelli (2011), which used diffusion approximations
4 to understand spatial and temporal dynamics. To determine the robustness of those diffusion-
5 based predictions, which make mathematical assumptions that may not be consistent with the
6 biology of *Wolbachia*-transfected mosquitoes, we examine dispersal patterns that assign higher
7 probabilities to long-distance (and very short-distance) dispersal. We ask how dispersal patterns
8 affect wave speed, wave shape, and the conditions for initiating an expanding wave. We use
9 these new, more robust predictions to propose guidelines for field deployment of dengue-
10 suppressing *Wolbachia*. This involves addressing new questions. For instance, Barton and Turelli
11 (2011) determined the minimum area over which *Wolbachia* must be introduced to initiate
12 spatial spread, but ignored the fact that near this critical size threshold, dynamics would be
13 extremely slow. Effective field deployment requires initiating multiple waves to cover a broad
14 area relatively quickly, given constraints on how many mosquitoes can be released. This requires
15 understanding how transient dynamics depend on initial conditions. We synthesize data-based
16 and model-based analyses of spatial spread to outline efficient strategies for area-wide
17 transformation of vector populations.

18

19 **Materials and Methods**

20 Our paper combines data analysis, used to support our assumption that introduced
21 *Wolbachia* infections produce bistable local dynamics, and mathematical analyses of bistable
22 dynamics. Our mathematical analyses focus on testing the robustness of predictions presented in
23 Barton and Turelli (2011). Below we first describe our data and the model used to analyze it. We
24 then describe the diffusion approximations and results from Barton and Turelli (2011) before
25 describing the alternative approximations and analyses used to test their robustness. Finally we
26 describe our approaches to approximating optimal release strategies.

27

1 **Data**

2 The *wMel* infection frequency data we analyze are a small subset of those collected
3 subsequent to first “Eliminate Dengue” field releases of *wMel*-infected *Ae. aegypti*, described in
4 Hoffmann et al. (2011). The releases occurred in early 2011 in two isolated towns, Gordonvale
5 (668 houses) and Yorkeys Knob (614 houses), near Cairns in northeast Australia. As described in
6 Hoffmann et al. (2011), Pyramid Estate (PE) is an area of Gordonvale separated from the town
7 center by a major highway, with roughly 100 m separating the nearest houses on either side.
8 Highways seem to inhibit *Ae. aegypti* migration (Hemme et al. 2010). The 2011 *wMel* releases
9 were restricted to the main part of Gordonvale; but as reported in Hoffmann et al. (2011), *wMel*-
10 infected mosquitoes were found in PE within months of the initial releases. The PE capture sites
11 were scattered over an area of houses on the order of 1 km² with traps roughly 100-500 m from
12 the nearest residences in our Gordonvale release area. As described in Hoffmann et al. (2011,
13 2014), infection frequencies were estimated using PCR of adults reared from eggs collected in
14 oviposition traps. Between late March 2011 and January 2015, 2689 adults were assayed in PE.
15 The data will be made available in an Appendix to this manuscript.

16

17 **Model: An isolated deme subject to immigration**

18 Barton and Turelli (2011) adapted the “island model” of Haldane (1930) to approximate the
19 rate of immigration of *Wolbachia*-infected individuals required to “flip” an isolated population
20 from uninfected to infected. In addition to approximating the critical migration rate, m , the
21 analysis produces an analytical approximation for the equilibrium infection frequency when the
22 immigration rate is too low to flip the recipient population to *Wolbachia* fixation. Assuming
23 complete CI, 100% frequency of *wMel* in Gordonvale (observed frequencies are about 96-98%,
24 Hoffmann et al. 2014), and one-way immigration into PE, Eq. (31) of Barton and Turelli (2011)
25 predicts that *wMel* should have reached fixation in PE if m , the fraction of individuals who were
26 new migrants each generation, exceeded $m^* = \hat{p}^2 / 4$. For $m < m^*$, the predicted *wMel*
27 equilibrium frequency, using a cubic approximation for local dynamics, is

1

$$2 \quad p^* = (\hat{p}/2) - \sqrt{(\hat{p}/2)^2 - m} < \hat{p}/2. \quad (1)$$

3

4 (this is a reparameterization of Eq. (31) of Barton and Turelli 2011). Hence, using \bar{p} , the long-
5 term average frequency of *wMel* in PE, to approximate p^* , the equilibrium described by (1), we
6 can approximate a lower bound for the unstable equilibrium, \hat{p} , as $2\bar{p}$.

7

8 **Model: Diffusion approximations and predictions**

9 The simplest spatial model relevant to understanding *Wolbachia* frequency dynamics in
10 space and time is a one-dimensional diffusion approximation:

11

$$12 \quad \frac{\partial p}{\partial t} = \frac{\sigma^2}{2} \frac{\partial^2 p}{\partial x^2} + f(p), \quad (2)$$

13 where $f(p)$ describes local dynamics and $p(x, t)$ denotes the infection frequency at point x and
14 time t . If we approximate the local bistable dynamics by the cubic

15

$$16 \quad f(p) = s_h p(1-p)(p - \hat{p}), \quad (3)$$

17 where s_h describes the intensity of CI, there is an explicit asymptotic traveling wave solution of
18 (2), given as Eq. 13 of Barton and Turelli (2011). Eq. (2), extended to two dimensions as
19 described by Eq. 22 of Barton and Turelli (2011), can be solved numerically to address transient
20 dynamics associated with local releases. In two dimensions, we interpret σ^2 as the variance in
21 dispersal distance per generation along any axis. (This implies that the average Euclidean
22 distance between the birthplaces of mothers and daughters is $\sigma\sqrt{\pi/2}$, assuming Gaussian
23 dispersal.) This model provides analytical predictions for wave speed and wave shape and
24 numerical conditions for establishing a spreading wave from a local introduction.

1 To more accurately approximate CI dynamics, Barton and Turelli (2011) replaced the cubic
 2 approximation (3) with the model of Schraiber et al. (2012)

$$3 \frac{dp}{dt} = f(p) = \frac{s_h p(1-p)(p - \hat{p})}{1 - s_f p - s_h p(1-p)}, \text{ with} \quad (4a)$$

$$4 \hat{p} = s_r/s_h = (s_f + s_v - s_f s_v)/s_h. \quad (4b)$$

6 (Eq. 4a assumes that the daily death rate for the infected individuals is $d_1 = 1$, so that time is
 7 measured in terms of the average lifetime of an infected individual.) As in (3), s_h measures the
 8 intensity of CI; s_f measures the net reduction in fitness caused by the *Wolbachia* infection. As in
 9 the discrete-time model of Turelli (2010), fitness cost may involve reductions of both fecundity
 10 and mean life length (viability), as measured by s_f and s_v , respectively; however, s_v enters the
 11 dynamics only through \hat{p} . Numerical integration can be used to compare the cubic-based
 12 analytical predictions with those produced by this more biologically explicit approximation. For
 13 fixed \hat{p} , the dynamics described by (4a) depend on whether fitness costs primarily involve
 14 viability or fecundity effects. The data of Hoffmann et al. (2014) suggest that fecundity effects
 15 may dominate.

17 **Wave speed.** Measuring time in generations, the predicted wave speed from (2) with cubic
 18 dynamics is

$$19 \quad c = \sigma \sqrt{s_h} (\frac{1}{2} - \hat{p}), \quad (5)$$

21 provided that $\hat{p} > 0$. This one-dimensional result also describes the asymptotic speed of a
 22 radially expanding wave in two dimensions (see Eqs. 23-25 of Barton and Turelli 2011). Barton
 23 and Turelli (2011) used numerical solutions of (2) to compare this speed prediction to the wave
 24 speed produced by (4a), which explicitly models the fast local dynamics associated with strong
 25 CI. The more realistic dynamics (4a) led to slightly faster wave propagation (as expected because

1 the denominator of $f(p)$ is less than one), with (5) underestimating the numerically calculated
2 speed by about 10% for complete CI.

3 .

4 **Wave width.** The explicit traveling-wave solution of (2) for cubic $f(p)$ provides a simple
5 description for the asymptotic wave width, the spatial scale over which infection frequencies
6 change. Defining wave width as the inverse of the maximum slope of infection frequencies
7 (Endler 1977), the diffusion approximation with cubic dynamics implies that the traveling wave
8 has width

9

$$10 \quad w = 1/\text{Max}(|\partial p/\partial x|) = 4\sigma/\sqrt{s_h}, \quad (6)$$

11

12 which becomes 4σ with complete CI, as in *Ae. aegypti*. The explicit solution that produces (6)
13 implies that with $s_h = 1$, the scaled wave (with space measured in units of σ) has shape
14 $1/[1 + \text{Exp}(-x)]$. Thus, infection frequencies increase from about 0.18 to 0.82 over 3σ . If steady
15 spread is observed in the field, we can use this approximation to estimate σ from spatial
16 infection-frequency data. These estimates can be compared to independent estimates from
17 release-recapture experiments or genetic data. We show below that relation (6) is relatively
18 robust to more realistic descriptions of local frequency dynamics and long-tailed dispersal.

19

20 **Wave initiation.** Finally, the diffusion approximation predicts the minimum area that must
21 be actively transformed to initiate deterministic spatial spread. Barton and Turelli (2011)
22 consider introductions over a circular area with initial infection frequency p_0 in the circle. This
23 initial state corresponds to rapid local establishment of a transinfection from intensive releases.
24 Hoffmann et al. (2011) showed that releases in isolated suburbs near Cairns produced *wMel*
25 frequencies over 80% within 12 weeks, about three *Ae. aegypti* generations. Fig 3 of Barton and
26 Turelli (2011) summarizes the diffusion predictions concerning the minimum radius of release
27 areas, measured in units of dispersal distance σ , needed to initiate a spreading wave. In their

1 analysis, the scaled critical radius, denoted R_{crit} , depends only on \hat{p} . As \hat{p} increases from 0 to
2 0.3, R_{crit} increases from 0 to about 3.5σ , then rapidly increases towards infinity as \hat{p} approaches
3 0.5, the approximate upper bound on \hat{p} consistent with spatial spread. Releases over areas
4 smaller than R_{crit} are predicted to fail, with the infection locally eliminated by immigration from
5 surrounding uninfected populations. Barton and Turelli (2011) used the Schraiber et al. (2012)
6 model (4) to assess the robustness of these cubic-based predictions to more realistic local CI
7 dynamics. Model (4) produced R_{crit} predictions within a few percent of those derived from the
8 cubic (see Fig 3 of Barton and Turelli 2011). Below, we contrast the diffusion predictions with
9 numerical results that account for faster local dynamics and alternative forms of dispersal.

10

11 **Mathematical analyses: Discrete-time, discrete-state analyses**

12 To explore the robustness of the diffusion predictions, we consider the simultaneous effects
13 of fast local dynamics, associated with complete CI, and long-tailed dispersal. To do this, we
14 replace the PDE approximation (2) with discrete-time, discrete-space (DTDS) models that
15 assume discrete generations and discrete patches in which the consequences of mating, fecundity
16 effects and CI occur and between which adult migration occurs.

17 **Discrete-time, discrete-state dynamics.** Let i denote a patch in one or two dimensions, let
18 $g(p) = p'$ denote a function that describes how mating, fecundity differences and CI transform
19 local infection frequencies between generations, and let $m(i, j)$ denote the probability that an
20 individual at location i after migration originated in location j . Assuming discrete generations in
21 which migration of newly eclosed individuals precedes local CI dynamics, the infection
22 frequencies among adults in each patch follow

23

$$24 \quad p(i, t+1) = \sum_j m(i, j)p'(j, t) \text{ or } p(i, t+1) = g\left[\sum_j m(i, j)p(j, t)\right]. \quad (7)$$

25 Our choice of patch spacing for these discretizations is discussed below.

1 We approximate local dynamics with the Caspari-Watson model (1959) which incorporates
 2 CI and fecundity effects (cf. Hoffmann and Turelli 1988; Weeks et al. 2007); setting $H = 1 - s_h$
 3 and $F = 1 - s_f$, and letting p denote the frequency of infected adults, the local dynamics are
 4 described by

$$5 \quad \Delta p = p' - p = \frac{s_h p(1-p)(p - \hat{p})}{1 - s_f p - s_h p(1-p)}, \text{ with} \quad (8a)$$

$$7 \quad \hat{p} = s_f/s_h. \quad (8b)$$

8 In this model, the condition for bistability (i.e., simultaneous local stability of $p = 0$ and $p = 1$) is
 9 $s_h > s_f > 0$, i.e., the (frequency dependent) benefit to the infection from CI must exceed its
 10 (frequency independent) cost, modeled as decreased fecundity.

11 **Alternative models of dispersal.** Following Wang et al. (2002), we compare results
 12 obtained using three models of dispersal: a Gaussian, denoted $G(x)$, versus two “long tailed”
 13 distributions, the Laplace (or reflected exponential), denoted $L(x)$, and the exponential square
 14 root (ExpSqrt), denoted $S(x)$. Letting σ denote the standard deviation of dispersal distances, our
 15 dispersal kernels in one dimension (proportional to the probability of moving distance x in one
 16 dimension) are

$$18 \quad G(x) = \text{Exp}[-x^2 / (2\sigma^2)] / \sqrt{2\pi\sigma^2}, \quad (9a)$$

$$19 \quad L(x) = \text{Exp}[-\sqrt{2x^2 / \sigma^2}] / \sqrt{2\sigma^2}, \text{ and} \quad (9b)$$

$$20 \quad S(x) = \sqrt{15 / (2\sigma^2)} \text{Exp}[-\sqrt[4]{120x^2 / \sigma^2}]. \quad (9c)$$

21
 22 These alternative dispersal models are illustrated in Fig 1. Our DTDS calculations used patch
 23 spacing of 0.5σ . We truncated the dispersal functions at $\pm 10\sigma$. We adjusted the variance
 24 parameter in our discrete calculations so that the actual standard deviation of the discrete

1 distribution was σ . In two dimensions, (x, y) , the dispersal models, generically denoted $f(z)$, were
2 implemented as $f\left(\sqrt{x^2 + y^2}\right)$.

3

4 **Fig 1. Alternative dispersal models with $\sigma = 1$.** The three models are: Gaussian (blue), Laplace
5 (green), and ExpSqrt (red) as described by (9). Each describes the probability, denoted $m(x)$ in
6 the figure, of moving distance x along any axis.

7

8 Taking logs of the densities, the tails of $G(x)$ decline as $-x^2$, whereas the tails of $L(x)$ and $S(x)$
9 decline as $-|x|$ and $-\sqrt{|x|}$, respectively, corresponding to successively higher probabilities of
10 long-distance dispersal. Denoting the random variables corresponding to these densities as G , L
11 and S , we have $P(|G| > 3\sigma) = 0.003$, $P(|L| > 3\sigma) = 0.014$ and $P(|S| > 3\sigma) = 0.022$. As Fig 1 shows,
12 higher probabilities of long-distance dispersal are accompanied by higher probabilities of short-
13 distance dispersal (e.g., $P(|G| < 0.5\sigma) = 0.383$, $P(|L| < 0.5\sigma) = 0.507$ and $P(|S| < 0.5\sigma) = 0.678$),
14 with corresponding medians for $|G|$, $|L|$ and $|S|$ of 0.67σ , 0.49σ and 0.28σ , respectively.

15 In two dimensions, we assume that dispersal is isotropic, with radial distribution given by
16 the kernels defined by Eq. 9, and scaled such that the standard deviation along any one axis is σ .
17 To approximate σ from experiments that estimate mean Euclidean dispersal distances, D , note
18 that the Gaussian produces $E(D_G) = \sigma\sqrt{\pi/2} \approx 1.25\sigma$, whereas for the Laplace and ExpSqrt, we
19 have $E(D_L) \approx 1.15\sigma$ and $E(D_S) \approx 0.94\sigma$, respectively. Thus, empirical estimates of average
20 Euclidean dispersal distance can imply values of σ that differ by over 30% depending on the
21 shape of the dispersal function, with longer tails implying higher values of σ . (Note that
22 statistical estimation of dispersal requires some assumption about the distribution of dispersal
23 distance.) We compare the predictions resulting from alternative dispersal models by holding
24 fixed the variance parameter σ , which is natural measure of dispersal distance for diffusion
25 approximations (see, for instance, the derivations in Haldane (1948), Slatkin (1973) or Nagylaki
26 (1975)).

27

1 **Near-optimal release strategies**

2 We analyze alternative release strategies using a combination of numerical diffusion
3 analyses, DTDS models and even simpler models that assume constant rates of radial spread
4 from release foci. Each analysis is described below along with the results it produces.

5 **Results**

6 **Empirical**

7 **Bistability.** PE was sampled for over two years after the releases stopped. The few capture
8 sites were scattered over an area of houses that is on the order of 1 km² with traps varying
9 between about 100 m and 500 m from the nearest residences in our release area. For over two
10 years, the *wMel* frequency in PE remained persistently low, but non-zero with $\bar{p} \approx 0.106$ ($N =$
11 2689, averaged over space and time, S. L. O'Neill, pers. comm.). (We found no evidence that
12 infection frequency varied with distance from the release area). For instance, a sample of 43 *Ae.*
13 *aegypti* from the week ending 9 January 2015 yielded an infection frequency of 0.07 [with 95%
14 binomial confidence interval (0.01, 0.19)]. From (1), a long-term average of 0.105 implies $\hat{p} \geq$
15 0.21. The persistence of a low infection frequency for over two years clearly demonstrates
16 regular immigration of infected individuals that has been unable to push the local PE population
17 past its unstable point. The fitness data from Hoffmann et al. (2014) and the transient dynamics
18 described in Hoffmann et al. (2011) suggest that \hat{p} for *wMel* near Cairns is likely to be at least
19 0.2. As discussed below, the dynamics of local releases within Cairns suggest that \hat{p} is unlikely
20 to be significantly above 0.3.

21
22
23 **Long-tailed dispersal.** Gordonvale and Yorkeys Knob are separated from other sizable
24 populations of *Ae. aegypti* by kilometers. Yet, Hoffmann et al. (2014) found consistent low
25 frequencies of uninfected individuals more than three years after *wMel* reached near-fixation,
26 despite no evidence for imperfect maternal transmission. Yorkeys Knob is less isolated than
27 Gordonvale and shows a significantly higher frequency of uninfected individuals, about 6%

1 versus 3%. Long-distance dispersal is the most plausible explanation for uninfected individuals
2 in Gordonvale and Yorkeys Knob – and the persistence of rare infected individuals at Pyramid
3 Estate. As shown below, long-tailed dispersal with complete CI can significantly alter some of
4 the diffusion-based predictions of Barton and Turelli (2011).

5
6 **Parameter estimates.** To predict propagation speed from (5), one needs estimates of σ , s_h
7 and \hat{p} . Both lab and field experiments indicate complete CI, i.e., $s_h \approx 1$ (Hoffmann et al. 2014).
8 Four lines of evidence suggest that \hat{p} is roughly 0.2-0.3 for *wMel* in *Ae. aegypti* populations near
9 Cairns: 1) the observed rate of increase of *wMel* during the introductions at Gordonvale and
10 Yorkeys Knob (Hoffmann et al. 2011, especially the mathematical analysis presented in the
11 Supplementary Information, see Figure S4), 2) the estimated 20% fecundity deficit for *wMel*-
12 infected females found by Hoffmann et al. (2014), 3) our crude lower bound of 0.21 for \hat{p}
13 obtained from the Pyramid Estate data and Eq. (1), and 4) the fate of releases in Cairns over
14 areas of different size (discussed below). Estimates of σ can be obtained either from mark-
15 release-recapture experiments (e.g., Russell et al. 2005) or from the shape of spreading waves, as
16 discussed below.

17 18 **Diffusion predictions for Cairns releases**

19 One of our primary aims is to understand the robustness of the Barton and Turelli (2011)
20 diffusion predictions. Rather than discuss generalities, we will focus on specific field releases. In
21 early 2013, three localized releases were performed within the city of Cairns. Releases were
22 made in three neighborhoods, Edgehill/Whitfield (EHW), Parramatta Park (PP), and Westcourt
23 (WC). The release areas were roughly 0.97 km² for EHW, 0.52 km² for PP, and only 0.11 km²
24 for WC. Infection frequencies quickly rose above 0.8 within all three release areas, and each
25 release area adjoined housing into which the *wMel* infection might plausibly spread. What
26 predictions emerge from the diffusion approximations?

1 Numerical predictions require estimates of σ and \hat{p} . Russell et al. (2005) performed a mark-
2 release-recapture experiment with *Ae. aegypti* using a release site abutting the 2013 EHW release
3 area. The mean absolute distance of recaptures from the release point was about 78 m. The
4 diffusion approximation assumes that dispersal is measured as the standard deviation of dispersal
5 distance along any axis. If we assume that dispersal distance is roughly Gaussian distributed with
6 mean 0 and standard deviation σ along each axis, the mean absolute dispersal distance is
7 $\sigma\sqrt{\pi/2}$ or about 1.25σ . With this assumption, the estimate from Russell et al. (2005) implies
8 $\sigma \approx 62 \text{ m}/(\text{generation})^{1/2}$. In general, however, release-recapture estimates tend to be
9 systematically lower than those based on genetic data (see, for instance, Barton and Hewitt 1985,
10 Fig 3). Moreover, estimates of dispersal distance for *Ae. aegypti* are extremely variable in time
11 and space. For instance, Harrington et al. (2005) found that repeated estimates of mean dispersal
12 distance in the same village in Thailand ranged from about $40 \text{ m}/(\text{generation})^{1/2}$ to about 160
13 $\text{m}/(\text{generation})^{1/2}$. Our theoretical predictions concerning the consequences of dispersal are best
14 interpreted as temporal averages, which are more likely to be accurately captured by indirect
15 estimates of average dispersal such as wave width (or genetic data describing the decline of
16 relatedness with distance). Given that direct estimates systematically underestimate average
17 dispersal in nature, we use $\sigma \approx 100 \text{ m}/(\text{generation})^{1/2}$ as a plausible estimate for Cairns. WE
18 recognize, however, that dispersal is likely to vary significantly with local conditions.

19 Assuming $\sigma \approx 100 \text{ m}/(\text{generation})^{1/2}$, Eq. (6) implies that if spatial spread is observed, the
20 wave width should be about 400 m. From Eq. (5), the corresponding wave speed is
21 $c = 100(1/2 - \hat{p}) \text{ m per generation (m/gen)}$. As argued above, \hat{p} is probably above 0.2. Thus, the
22 maximum predicted speed is about 30 m/gen. However, if \hat{p} is as high as 0.35, predicted speed
23 falls to 15 m/gen. Assuming about 10 *Ae. aegypti* generations per year near Cairns, these crude
24 estimates indicate that *wMel* spread in *Ae. aegypti* is likely to be on the order of 150-300 m/year
25 – two or three orders of magnitude slower than the spread of *wRi* in California and eastern
26 Australia *D. simulans* (100 km/year). Yet repeated estimates of dispersal distances for various
27 *Drosophila* species suggest that natural dispersal distances are at most 5-10 times greater for *D.*

1 *simulans* than for *Ae. aegypti* (e.g., Dobzhansky and Wright 1943; Powell et al. 1976; McInnis et
2 al. 1982). The critical difference between the speeds associated with these exemplars of
3 *Wolbachia* spread is unlikely to be dispersal, but more probably the bistability of *wMel* dynamics
4 in *Ae. aegypti* versus the monostability of *wRi* dynamics. Monostability allows relatively rare
5 human-mediated, long-distance dispersal to greatly enhance spatial spread, as described, for
6 instance, by “structured diffusion” models (Shigesada and Kawasaki 1997, Ch. 5).

7 Whether spatial spread occurs with bistability depends on the size of the release area, the
8 initial frequency produced in the release area (p_0), and \hat{p} . From Fig 3 of Barton and Turelli
9 (2011) with $p_0 = 0.8$, if \hat{p} were as large as 0.35, the minimum radius of a circular release needed
10 to produce an expanding wave would be on the order of 4σ , implying a minimal release area of
11 about 0.5 km^2 (assuming $\sigma \approx 100 \text{ m}/(\text{generation})^{1/2}$). Replacing the cubic in (2) with the
12 Schraiber et al. (2012) description of CI dynamics (4), Barton and Turelli (2011) showed that the
13 minimal radius with $\hat{p} = 0.35$ falls from about 4σ to about $2.8\text{-}3.5\sigma$, with the value depending on
14 whether *wMel*-infected *Ae. aegypti* lose fitness primarily through fecundity (as the data of
15 Hoffmann et al. 2014 suggest), which produces 2.8σ , or viability, which produces 3.5σ . The
16 smaller values (from Schraiber et al. 2012) imply minimal release areas of about $0.25\text{-}0.38 \text{ km}^2$
17 (the lower value assumes only fecundity effects). In contrast, if \hat{p} were as small as 0.2, the
18 minimum radius falls to about 2σ for both the cubic model and Schraiber et al. (2012) dynamics
19 (with either fecundity or viability effects), corresponding to a minimal area of about 0.13 km^2 .

20 Table 1 summarizes our diffusion-based predictions. Note that according to these analyses,
21 the releases at EHW and PP should certainly lead to spatial spread, but the WC release is close to
22 minimal release area even if \hat{p} is as small as 0.2. Next we address the robustness of these
23 predictions to long-tailed dispersal and patchy spatial distributions.

24
25

1 **Table 1. Diffusion-based predictions for spatial spread.**

2

3

4

Unstable point	Speed (m/gen)	Width (m)	Minimum Release Area (km ²)
$\hat{p}=0.2$	30	400	0.13
$\hat{p}=0.35$	15	400	0.25-0.38 ^a (0.5)

5

6 These predictions assume $\sigma \approx 100$ m and $0.2 \leq \hat{p} \leq 0.35$. They are based on Eq. 5, Eq. 6 and Fig
 7 3 of Barton and Turelli (2011).

8 ^aThe smaller prediction (0.25) is derived with Schraiber et al. (2012) CI dynamics (4a) assuming
 9 that *wMel* reduces only the fecundity of *Ae. aegypti* (i.e., $s_r = s_f$ in 4b), the larger result (0.38)
 10 assumes that *wMel* reduces only viability. The cubic model produces the still larger value (0.5).

11

12 **Consequences of long-tailed dispersal and rapid CI dynamics: DTDS robustness analyses**
 13 **of diffusion results. Wave speed.** We initially calculated wave speed in a one-dimensional
 14 spatial array, then as in Barton and Turelli (2011), we checked the results with two-dimensional
 15 calculations. To disentangle the effects of non-Gaussian dispersal from the effects of fast local
 16 dynamics, we contrast results obtained assuming complete CI ($s_h = 1$), as observed with *wMel*-
 17 infected *Ae. aegypti*, with results assuming weak CI ($s_h = 0.2$). Fig 2 compares the numerically
 18 approximated wave speeds to the analytical prediction, $c = \sigma\sqrt{s_h}(\frac{1}{2} - \hat{p})$, from the diffusion
 19 approximation with cubic dynamics. The left panel shows that with relatively slow local
 20 dynamics ($s_h = 0.2$), the cubic diffusion approximation is accurate and robust to the shape of the
 21 dispersal function. This is expected from the derivation of approximation (2) as a limit of
 22 discrete-time, discrete-space dynamics (Haldane 1948; Nagylaki 1975). The derivation explicitly
 23 invokes slow local dynamics and limited dispersal, retaining only the variance of dispersal
 24 distances in the quadratic approximation. The $s_h = 0.2$ results have two other notable features.
 25 First, despite the overall accuracy of approximation (5), we see that ExpSqrt dispersal slightly
 26 slows propagation. This can be understood in terms of the lower median dispersal distance and
 27 the fact that with bistability, rare long-distance dispersal is effectively eliminated and hence not
 28 effective at pushing the wave forward. This distinguishes bistable spatial dynamics from those
 29 with 0 as an unstable equilibrium. For such systems, long-tailed dispersal can produce

1 accelerating waves (see Supporting Information Appendix A for references and comparison of
2 bistable versus Fisherian wave speeds). Moreover, geographic spread associated with spatially
3 non-contiguous, successful long-distance colonization events (cf. Shigesada and Kawasaki 1997,
4 Ch. 5), can greatly exceed predictions based on average dispersal distances. Second, note that as
5 \hat{p} approaches 0.5, the analytical approximation starts to underestimate wave speed. As described
6 by Barton and Turelli (2011), this reflects the fact that the cubic model produces the threshold \hat{p}
7 ≤ 0.5 for spatial spread, whereas models more accurately describing CI and fitness costs, such as
8 (4a) and (8a), predict spatial spread with \hat{p} slightly above 0.5.

9
10 **Fig 2. Wave speed.** Speed calculated from DSDT analyses compared to the cubic-based
11 diffusion prediction, $c = \sigma\sqrt{s_h}(\frac{1}{2} - \hat{p})$, as a function of \hat{p} , for $s_h = 0.2$ (left) and $s_h = 1$ (right).
12 The green dots were produced with Gaussian dispersal, blue with Laplace and black with
13 Exponential Square root (ExpSqrt).

14
15 The right panel of Fig 2 ($s_h = 1$) shows that faster local dynamics accentuate both
16 phenomena seen with $s_h = 0.2$: slower speed with more long-tailed dispersal and underestimation
17 of observed speed as \hat{p} approaches 0.5. With complete CI and plausible \hat{p} (*i.e.*, $0.2 \leq \hat{p} \leq 0.35$),
18 observed speed closely follows the cubic-based diffusion prediction with Gaussian dispersal, but
19 is reduced by about 10% for Laplace dispersal and by much more (25-40%) for ExpSqrt
20 dispersal. A simple interpretation is that long-tailed dispersal is associated with smaller median
21 dispersal distances. Long-distance migrants are effectively “wasted” in that they cannot initiate
22 local spread.

23 Appendix A provides a more complete description of the consequences of alternative
24 dispersal models on wave speed under bistable versus monostable local dynamics, including the
25 consequences of finite population size at the front on wave propagation. It also clarifies the
26 distinction between “pulled” and “pushed” waves.

1

2 **Wave width.** Under the diffusion model with cubic dynamics, the predicted wave width is
3 $w \approx 4\sigma \sqrt{s_h}$ (6). Fig 3 compares this prediction with the results obtained from DTDS with
4 Caspari-Watson dynamics and alternative dispersal models. With relatively slow local dynamics
5 ($s_h = 0.2$), Panel A shows that the cubic-diffusion prediction remains accurate for all three
6 dispersal models, analogous to the results for wave speed illustrated in Fig 2A. ExpSqrt dispersal
7 slightly reduces wave width, presumably reflecting the lower median dispersal. As with wave
8 speed, $s_h = 1$ produces larger departures from the cubic-diffusion prediction and much greater
9 effects of dispersal shape. However, for plausible values of \hat{p} (i.e., $0.2 \leq \hat{p} \leq 0.35$), the observed
10 width remains within about 15% of prediction (6) for Gaussian and Laplace and very close to the
11 prediction for ExpSqrt.

12

13

14 **Fig 3. Wave width.** Wave width as a function of \hat{p} calculated using discrete-time, discrete-
15 space (DTDS) analyses with alternative dispersal models. The dots from the DTDS analyses are
16 compared to the diffusion prediction ($w = 1/\text{Max}(|\partial p/\partial x|) = 4\sigma/\sqrt{s_h}$, red line) for $s_h = 0.2$ (left)
17 and $s_h = 1$ (right). The green dots were produced with Gaussian dispersal, blue with Laplace and
18 black with Exponential Square root (ExpSqrt).

19

20 **Wave initiation: Critical radius ρ_{crit} .** Fig 3 of Barton and Turelli (2011) showed how R_{crit} ,
21 the minimal radius of an introduction needed to initiate spread (measured in units of the dispersal
22 parameter σ), depends on \hat{p} and p_0 under the diffusion approximation. It contrasts the
23 predictions for cubic dynamics versus Schraiber et al. (2012) *Wolbachia* dynamics (Eq. 4). Fig 4
24 compares those predictions to DTDS results under Caspari-Watson *Wolbachia* dynamics (Eq. 8).
25 The key result is that long-tailed dispersal produces smaller critical radii, and the effect of long-
26 tailed dispersal increases as \hat{p} increases. This result is complementary to the wave-speed results.

1 With longer-tailed dispersal, more individuals move very little so that the median dispersal falls,
2 making it easier to establish a wave (but the resulting wave moves more slowly). The
3 discrepancies between the diffusion results with Schraiber et al. (2012) dynamics and the DTDS
4 results for Gaussian dispersal are mainly attributable to the fact that the Schraiber et al. (2012)
5 results assume only viability costs, which produces slower dynamics and requires larger
6 introductions, than if one assumes fecundity costs, as done in the DTDS Caspari-Watson model
7 (see Table 1).

8
9
10 **Fig 4. Critical radius, R_{crit} , assuming complete CI and Caspari-Watson dynamics.** The
11 upper points reproduce the diffusion results from Barton and Turelli (2011) with cubic (red
12 curve) and Schraiber et al. (2012) CI dynamics. The red curve shows the cubic-diffusion
13 predictions with $p_0 = 0.8$, the large blue dots are the cubic with $p_0 = 0.6$. The small red (blue) dots
14 are produced by the diffusion analysis of Schraiber et al. (2012) CI dynamics with $p_0 = 0.8$ ($p_0 =$
15 0.6), assuming only viability fitness costs. The lower points and curves show our DTDS
16 predictions as a function of \hat{p} and the initial infection frequency (p_0) with alternative dispersal
17 models. The lower lines correspond to $p_0 = 0.8$ with Gaussian (green), Laplace (blue) and
18 ExpSqrt (black) dispersal. The points above and below these lines correspond to $p_0 = 0.6$ and p_0
19 $= 1$, respectively

20

21 There are two striking results concerning the DTDS-derived values of R_{crit} . First, like the
22 wave-width results, the critical radii are relatively insensitive to the dispersal model. Second,
23 however, unlike the wave-width results, the critical radii are significantly different and smaller
24 than those produced by the diffusion approximation. Barton and Turelli (2011) showed that the
25 Schraiber et al. (2012) dynamics produced smaller R_{crit} values than the cubic model, even if

1 fitness costs were purely based on reduced viability. Reduced fecundity, as assumed in the
2 Caspari-Watson model, accelerates the local dynamics and hence allows much smaller
3 introductions to initiate a traveling wave. Even with $\hat{p} = 0.35$, introductions with $p_0 = 0.8$ will
4 succeed as long as $R_1 \geq 2.5\sigma$ (3.0σ) with ExpSqrt (Gaussian) dispersal.

5

6 **DTDS predictions for Cairns releases.** Our robustness analyses of the wave-width
7 predictions emerging from the cubic-diffusion model indicate that σ can be reliably estimated
8 from observed widths of traveling waves of *Wolbachia* infections. In contrast, our wave-speed
9 analyses suggest that given an estimate of σ , the predicted wave speed depends significantly on
10 the shape of dispersal with plausible speeds that may be on the order of 20-30% below the cubic-
11 diffusion prediction $c = \sigma\sqrt{s_h}(\frac{1}{2} - \hat{p})$.

12 Our final prediction concerns spatial spread from individual localized releases. As shown in
13 Fig 4, the critical release radius for spread depends on: 1) \hat{p} , the unstable point; 2) p_0 , the initial
14 infection frequency produced within the release areas; 3) the shape of the dispersal function; and
15 4) σ , dispersal distance. As dispersal becomes more long-tailed (moving from Gaussian to
16 ExpSqrt), the critical radius of the initial introduction decreases. If we assume that $\hat{p} = 0.3$ and
17 $p_0 = 0.8$, R_{crit} is about 2.61σ if dispersal is Gaussian, but falls to about 2.51σ (or 2.16σ) if
18 dispersal is Laplace (or ExpSqrt). Hence, for each of the three release areas in Cairns, we can ask
19 what is the maximum σ consistent with our deterministic predictions for spatial spread. Given
20 that spread occurs only if the release area exceeds $\pi R_{crit}^2 \sigma^2$, for each release area, we can
21 approximate an upper bound on σ consistent with spatial spread by

22

23

$$24 \quad \sigma < \sqrt{(\text{release area})/(\pi R_c^2)}. \quad (10)$$

25

26 Table 2 presents these upper bounds on σ associated with the three 2013 release areas in central
27 Cairns for a plausible range of \hat{p} .

28

1
2
3
4
5
6

Table 2. Predicted maximum σ (in meters) consistent with spatial spread.

Location	\hat{p}	Gaussian	Laplace	ExpSqrt
Westcourt (0.11 km ²)	0.2	92	95	115
	0.25	81	84	101
	0.3	72	74	87
	0.35	62	64	73
Parramatta Park (0.52 km ²)	0.35	135	140	160
Edge Hill/Whitfield (0.97 km ²)	0.35	184	191	218

7
8
9

These prediction, based on inequality (10), assume that assuming that $p_0 = 0.8$ and $0.2 \leq \hat{p} \leq 0.35$.

10
11
12
13
14
15
16
17

Given that very few empirical estimates of σ for *Aedes aegypti* exceed 100 m, these results suggest that spatial spread should certainly be observed for the Edge Hill/Whitfield and Parramatta Park releases. The prediction for Westcourt is more ambiguous. Note that from Table 1, our diffusion predictions with $0.2 \leq \hat{p} \leq 0.35$ indicated a minimum release area of 0.14 km². This lower bound assumes $\sigma = 100$ m and $\hat{p} = 0.2$. Thus the diffusion analyses suggested probable failure of the Westcourt release. In contrast, as shown in Fig 4, our DTDS analyses indicate that the Westcourt release area may be near the lower limit for spread, with the outcome depending critically on the exact values of σ and \hat{p} .

18
19
20
21
22
23
24

Empirically testing these predictions concerning minimal release areas is confounded by the fact that dynamics very close to the critical values for spread are expected to be slow. Assuming that $\hat{p} = 0.25$, if the release area is 10% (5%) smaller than the critical value, the time for collapse is on the order of 15-20 (20-25) generations, roughly two years. Conversely, if the release area is only 10% (5%) larger than the critical area, the time scale for appreciable spatial spread is also on the order of 15-20 (20-25) generations. In contrast, release areas twice as large as necessary should produce appreciable spread in only 10-15 generations; whereas release areas only half as

1 large as needed should essentially collapse in 10-15 generations. These calculations motivated
2 our analyses presented below of “optimal” release sizes aimed at area-wide coverage within a
3 few years.

4

5 **Consequences of patchy population structure**

6 We have assumed throughout a uniform population density and dispersal rate. In reality, habitat
7 heterogeneity may slow – or stop – the spread of a wave. If increase is expected from low
8 frequencies, then a few long-range migrants can take the infection beyond a local barrier. We
9 expect this has happened repeatedly with the observed spread of *wAu* and *wRi* in *Drosophila*
10 *simulans* (cf. Coyne et al. 1982; Coyne et al. 1987; Kriesner et al. 2013). Similarly, many
11 episodes of successful long-distance dispersal and local establishment must underlie the global
12 spread of *Aedes aegypti* out of Africa (Brown et al. 2011). However, bistability, as expected for
13 the *wMel* infection in *Ae. aegypti*, implies that infection spread can be stopped indefinitely, as
14 seems to be the case with Pyramid Estate/Gordonvale near Cairns. Barton and Turelli (2011, Eq.
15 20) gave a simple result that shows how a gradient in population density alters wave speed:
16 regardless of the detailed dynamics, a gradient in log density will slow (or accelerate) a travelling
17 wave by $\sigma^2 d(\log(\rho(x)))/dx$, where $\rho(x)$ denotes the population density at x . However, such a
18 gradient must be sustained over a sufficient distance. Local heterogeneities, such as those due to
19 the spacing between discrete demes (e.g., individual households harboring *Ae. aegypti*), have a
20 negligible effect if they are over a shorter scale than the width of the wave (Barton 1979, p. 357).

21 In contrast, when the wave encounters a significant barrier, such as the highway separating
22 Pyramid Estate from Gordonvale, we can understand wave stopping either in terms of sharp
23 breaks in density, as considered in Fig 6 of Barton and Turelli (2011), or in terms of migration
24 from an infected population into an uninfected population. The latter produces a lower bound on
25 immigration rate needed to “flip” the uninfected population past the unstable point, as discussed
26 above Eq. 1.

27

1 **Near-optimal release strategies**

2 We seek conditions under which releases of disease-suppressing *Wolbachia* transinfections
3 achieve area-wide control of a disease such as dengue (cf. Ferguson et al. 2015) by transforming
4 a significant fraction of the vector population, say 80%, in a relatively rapid period, say two to
5 four years (on the order of 20-40 generations), while releasing as few *Wolbachia*-infected vectors
6 as possible. We consider several questions associated with the optimizing the timing, spacing
7 and intensity of releases. First, we contrast pulsed releases, over a time scale of very few vector
8 generations, with prolonged low-intensity releases. Second, we consider optimizing the spacing
9 and intensity of releases, as quantified by three parameters: a) local initial infection frequencies
10 after releases, b) areas of local releases, and c) the spacing of releases. Third, given that
11 optimization requires knowing parameters that can only be approximated, we consider the
12 consequences of non-optimal releases.

13

14 **Timing of releases: pulse versus gradual introduction.** With bistable dynamics, the
15 frequency of an infection (or allele) must be raised above a critical threshold, \hat{p} , over a
16 sufficiently large area to initiate spread. What is the most efficient way to establish an infection?
17 At one extreme, the frequency could be raised essentially instantaneously to some $p_0(x)$; if $p_0 > \hat{p}$
18 over a large enough region (cf. Fig 4), the infection will spread. At the other extreme, there
19 might be a gradual introduction, described by a local introduction rate $m(x)$, sustained until
20 deterministic spread is initiated. If this input is sufficiently high over a sufficiently large region,
21 the infection will be locally established and spread. Between these extremes, releases might be
22 sustained for a set period of many months or a few years. Supporting Information Appendix B
23 investigates conditions for local establishment and wave initiation, providing analytical results
24 for a single deme and for a point source of introduction in one dimension, and numerical results
25 for two dimensions. We show that it is most efficient to raise infection frequency rapidly, in a
26 brief pulse, rather than making gradual introductions. This accords with the intuition that it is
27 most efficient to raise the frequency as quickly as possible above the threshold \hat{p} : this

1 maximizes the reproductive value of introduced individuals. The principle is simple; during
2 gradual introductions, until local infection frequencies exceed \hat{p} , the introduced infected
3 individuals are systematically eliminated by deterministic selection that dominates the weaker
4 (frequency-dependent) force of CI at low *Wolbachia* frequencies. Assuming that releases quickly
5 drive the local infection frequency to a value p_0 sufficient to initiate spatial spread, we ask how
6 long it might take to cover a large area and what spatial patterns of release minimize the time to
7 reach a desired coverage.

8

9 **Spacing and intensity of releases.** We start with idealized analyses, then discuss their
10 relative robustness and the effects of environmental heterogeneity. Consider an area with a
11 relatively uniform vector density. What is the optimal release strategy? The calculations in
12 Appendix B show that for a given number of mosquitoes, the best strategy is to release a short
13 pulse, *i.e.*, to essentially instantly produce a local infection frequency sufficient to initiate a
14 wave. Obviously there are practical constraints on numbers that can be released, as well as
15 density-dependent effects, that limit the rate of local transformation. However, empirical results
16 of Hoffmann et al. (2011) demonstrate that patches on the order of 1 km² can be converted to
17 relatively high *Wolbachia*-infection frequencies, on the order of 0.8, within two or three months.
18 For simplicity, we focus on releasing *Wolbachia*-infected mosquitoes in circular areas of radius
19 R_I that will form expanding waves. Because the expansion rate approaches zero as the release
20 radius approaches the critical size threshold needed to produce an expanding wave, R_I must
21 exceed this critical size. We assume that because of limitations associated with density regulation
22 and constraints on numbers released, the highest initial frequency, p_0 , that can plausibly be
23 achieved in each release area is $p_{\max} < 1$. We consider laying out release areas in a uniform grid
24 with spacing D between the centers of each release.

25 We envision expanding waves from each release. When the waves meet, the radius of each
26 infected patch is $D/2$ and the fraction of the space occupied by *Wolbachia*-transformed
27 mosquitoes is $\pi/4 = 0.785$ (*i.e.*, $\pi(D/2)^2/D^2$), or roughly 80%. If the waves were instantly moving

1 at the asymptotic speed c , they would meet in $(D/2 - R_1)/c$ time units. The actual time will be
2 slower because the infection frequency must rise in the release area and the proper wave shape
3 establish. Given that we can control p_0 ($\leq p_{\max}$), R_1 , and D , we can ask: what values of these three
4 parameters produce waves that meet in a minimum time for a fixed number of mosquitoes
5 released – and what is that time? Alternatively, we can ask what is the minimum number of
6 mosquitoes that must be released to produce advancing waves that meet within a fixed time?
7 Given practical constraints on achieving specific values for p_0 , R_1 , and D , we then consider how
8 sensitive our results are to these parameters and to model assumptions concerning dynamics and
9 dispersal.

10

11 **Empirically based approximations for area-wide coverage**

12 Before addressing these questions with detailed dynamic models, we provide informative
13 approximations from empirical results. From the data reported in Hoffmann et al. (2011) and
14 Hoffmann et al. (2014), we know that releases of wMel-infected *Aedes aegypti* can be used to
15 stably transform areas with radius roughly $R_1 = 400$ m. A *Wolbachia* frequency of about 80%
16 within such release areas can be achieved in about 10 weeks (under three generations) by
17 releasing weekly a number of adults on the order of 50-100% of the resident adult population
18 (Hoffmann et al. 2011; Ritchie et al. 2013). Our theoretical analyses above and in Barton and
19 Turelli (2011) suggest that rates of spatial spread are likely to be habitat dependent. But in
20 relatively uniform habitats comparable our release areas near Cairns with $\sigma \approx 100$
21 $\text{m}/(\text{generation})^{1/2}$ and $\hat{p} \approx 0.25-0.3$, we expect wave speeds on the order of 10-20 m per month.

22 To understand the consequences of slow spatial spread, we initially consider dividing the
23 target region into non-overlapping $D \times D$ squares. We will determine the value of D that
24 achieves about 80% coverage over the desired period. Suppose that at the center of each square,
25 we release *Wolbachia*-infected mosquitoes over a circle of radius R_1 . Assume that each release
26 initiates a wave moving c meters per generation (roughly per month). If we want the expanding

1 circles to hit the edges of the $D \times D$ squares within T generations, the wave front must move a
 2 distance $D/2 - R_1$ in T generations. Hence, the distance between adjacent centers must be

$$3 \quad D = 2(R_1 + cT). \quad (11)$$

5
 6 The fraction, F , of the target area that must be actively transformed to achieve $\pi/4$ coverage in T
 7 generations is $F = \pi R_1^2 / D^2$, where D is given by (11). Thus,

$$8 \quad F = \pi R_1^2 / [4(R_1 + cT)^2]. \quad (12)$$

10
 11 Table 3 shows how F depends on time (T , in generations), wave speed per generation (c), and the
 12 initial release radius (R_1). The target times correspond roughly to one-to-four years. These
 13 approximations make sense only if the initial frequency in the release area is high enough that
 14 the asymptotic wave speed is reached within a few generations. They imply that for relatively
 15 homogeneous target areas consistent with steady spatial spread, roughly 80% can be covered in
 16 three or four years with initial releases of 0.5-1 km² that cover about 10-30% of the target.
 17 Comparable results are obtained below from explicit dynamic models for wave initiation and
 18 spread.

19
 20

21 **Table 3. Fraction of the target area that must be actively transformed to produce about**
 22 **80% ($\pi/4$) coverage in T generations.**

23 24 25 26 R_1 (area)	40 generations	30 generations	20 generations	10 generations
400 m (0.5 km ²)	0.09-0.20	0.13-0.26	0.20-0.35	0.35-0.50
560 m (0.99 km ²)	0.13-0.27	0.18-0.33	0.27-0.43	0.43-0.57

27 These calculations assume wave speed $c = 10-20$ m/generation starting from initial releases in
 28 circles of radius R_1 that produce local infection frequencies p_0 near 1.

29

1 To completely cover a region as quickly as possible, a regular grid of releases is not optimal.
2 Fig 5 shows how rows of releases with the centers offset between adjacent rows reduces the
3 distance each wave must travel by $D/\sqrt{2} - 5D/8 \approx 0.08D$. (Note that with the release
4 configuration shown in Fig 5, when the radii of the expanding waves reach $5D/8$, the entire target
5 area has been transformed.) The empirical relevance of such idealized release spacings is
6 considered in the Discussion.
7

8 **Fig 5. Optimal spacing.** The green circles within the $D \times D$ squares represent release areas with
9 radii R_1 . If the release areas were laid out on a regular grid, each expanding wave would have to
10 travel to the corner of the enclosing square, a distance of $D/\sqrt{2} - R_1$, to transform the entire
11 target area. In contrast, by offsetting the release centers between adjacent rows, as illustrated,
12 each wave must travel only $5D/8 - R_1$ for area-wide transformation.
13

14 **Model-based approximations**

15 Next, we reconsider the times to achieve roughly 80% coverage using explicit models for
16 temporal and spatial dynamics. With explicit dynamics we can address various questions
17 involving, for instance, optimal size and spacing of release areas and optimal initial frequencies
18 in the release areas. Release areas have a major impact on subsequent dynamics. For releases
19 near the minimal sizes required to initiate spread (cf. Fig 4), dynamics will be extremely slow. In
20 contrast, our calculations above assume that asymptotic wave speed is reached essentially
21 instantaneously. Assuming Caspari-Watson dynamics with alternative dispersal models, we use
22 the DTDS approximations (7) to describe optimal release strategies under different constraints.
23

24 **Optimal spacing and sizes of releases.** For these calculations, we assume that releases
25 occur in a fixed fraction, ρ , of the target area and that the initial *Wolbachia* frequency within the
26 release areas is p_0 . To understand fully how mosquito releases translate into local infection
27 frequencies, density regulation must be understood. Instead, we consider ρ and p_0 as simple

1 proxies for release effort. As above, we assume that release areas are circles of radius R_1 set at
2 the centers of $D \times D$ squares that cover the target area. Given ρ , the spacing D dictates the radii,
3 R_1 , of the releases, with $R_1 = D\sqrt{\rho/\pi}$. For fixed ρ , we seek the spacing D (or equivalently the
4 release area) that minimizes the time until the waves meet (covering $\pi/4$ of the target area). The
5 minimal time is denoted T_{\min} .

6 Assuming releases over 20% of the target area ($\rho = 0.2$) with initial infection frequencies,
7 p_0 , of 0.6 or 0.8 in each release area, Table 4 presents optimal spacing for releases and the
8 number of generations to reach 80% coverage for two plausible values of \hat{p} . What seems most
9 notable is that for these parameters, the optimal release radii are only about 30-45% larger than
10 the minimum radii needed to initiate spatial spread. With “optimal” spacing, 80% coverage is
11 predicted in about 1.25-3.5 years, assuming about 10 generations per year. The values of T_{\min} are
12 considerably smaller than those reported in Table 3, and the critical difference is that the release
13 areas are considerably smaller. Table 3 assumes $\sigma = 100$ m, so the release sizes are fixed at $R_1 =$
14 4 and 5.6. The shorter times in Table 4 are associated with the fact that in principle smaller
15 releases will suffice to start waves that relatively quickly approach their asymptotic speed.

16
17
18

1 **Table 4. Optimal spacing of releases.**

2

3

4

5

6

7

$p_0 = 0.6$		$\hat{p} = 0.2$			$\hat{p} = 0.3$			
Dispersal	D	R_l	R_{crit}	T_{min}	D	R_l	R_{crit}	T_{min}
Gaussian	13.06	3.30	2.48	17.60	16.26	4.10	3.19	30.22
Laplace	12.21	3.08	2.35	17.95	16.22	4.09	3.06	31.13
ExpSqrt	11.30	2.85	1.99	19.54	15.11	3.81	2.64	34.87

$p_0 = 0.8$		$\hat{p} = 0.2$			$\hat{p} = 0.3$			
Dispersal	D	R_l	R_{crit}	T_{min}	D	R_l	R_{crit}	T_{min}
Gaussian	11.26	2.86	2.05	14.17	13.43	3.39	2.61	24.26
Laplace	10.25	2.60	1.97	14.57	13.39	3.38	2.52	25.09
ExpSqrt	9.34	2.36	1.62	16.25	12.18	3.07	2.16	28.59

8 All distances are measured in units of σ . Assuming releases over 20% of the target area (i.e., $\rho =$
 9 0.2 and $p_0 = 0.6$ or 0.8), we compare the spacing, D (distance between adjacent release centers),
 10 that produces the shortest time (in generations), T_{min} , required to reach 80% coverage as a
 11 function of p_0 , initial infection frequency in release areas, \hat{p} and dispersal shape. The initial
 12 radius of these optimal releases, $R_l = D\sqrt{\rho/\pi}$, is compared to the minimum radius, R_{crit} ,
 13 required to initiate an expanding wave for the specified p_0 and \hat{p} .

14

15 Table 4 shows that T_{min} depends only weakly on the shape of dispersal. As expected from
 16 our speed calculations, long-tailed dispersal leads to longer wait times. Two factors contribute to
 17 this, the differences in wave speed demonstrated in Fig 2 and the differences in the optimal
 18 spacing. With longer dispersal tails, wave speed slows down, but the optimal spacing is closer
 19 (because smaller release radii suffice to initiate spread), and these effects partially cancel. In
 20 contrast, as \hat{p} increases from 0.2 to 0.3, T_{min} increases by 70-80%, whereas the analytical
 21 prediction $c = \sigma\sqrt{s_h}(\frac{1}{2} - \hat{p})$ and the numerical results in Fig 2 indicate that wave speed should
 22 decrease by only about 50%, at most. The additional factor explaining the discrepancy is that
 23 larger releases are needed, producing larger spacing, D , so that the waves must travel farther to

1 meet. Table 4 also predicts how T_{\min} varies with the number of infected mosquitoes released, as
2 measured by p_0 . As expected, the critical spacing, D , and the minimal time, T_{\min} , fall as initial
3 frequencies rise. For instance, with Gaussian dispersal and $\hat{p} = 0.3$, (D, T_{\min}) fall from (13.06,
4 17.60) with $p_0 = 0.6$ to (10.74, 14.25) with $p_0 = 0.8$ and to (9.36, 12.03) with $p_0 = 1.0$. Overall,
5 decreasing p_0 from 0.8 to 0.6 leads to lengthening T_{\min} by a factor of 1.20-1.25.

6

7 **Optimal distribution: release area, ρ , versus initial frequency, p_0 .** Optimization depends
8 on constraints. Above we assume that ρ and p_0 have been chosen, then seek the optimal spacing
9 (or equivalently the optimal sizes for the individual release areas), conditioned on ρ , the total area
10 over which releases will occur. An alternative is to assume that available resources dictate the
11 number of mosquitoes that can be released, then ask whether it is more efficient to produce a low
12 initial frequency over a large area or a higher frequency over a smaller area. In general, we
13 expect that achieving a frequency of 0.45 requires less than half the effort required to achieve 0.9
14 for at least two reasons. First, density-dependence is likely to produce diminishing returns from
15 very intensive releases (Hancock et al. 2016); and second, very high frequencies can only be
16 achieved with repeated releases, which are less efficient than more intense releases over shorter
17 periods. Nevertheless, if we view that product ρp_0 as proportional to total release effort, it is
18 instructive to ask for a fixed ρp_0 what p_0 achieves 80% coverage as quickly as possible?

19 Using all three dispersal models and $\hat{p} = 0.2$ or 0.3, Fig 6 plots the minimal time to achieve
20 80% cover as a function of p_0 assuming $\rho p_0 = 0.2$. The results indicate that releases producing
21 initial frequencies between roughly 0.5 and 0.8 are essentially equivalent, with coverage times
22 varying less than 10%. In contrast, the considerable additional effort required to produce $p_0 \geq 0.9$
23 yields slightly slower rather than faster coverage. Conversely, reaching only $p_0 = 0.04$ -0.5
24 requires significantly larger optimal release areas and yields slower coverage. For instance, with
25 Laplace dispersal, $\hat{p} = 0.3$, and $\rho p_0 = 0.2$, T_{\min} is achieved with $R_1 = 4.10$ for $p_0 = 0.7$ but $R_1 =$
26 5.84 for $p_0 = 0.5$, corresponding to roughly doubling the release areas. These results suggest that
27 releases should aim for initial *Wolbachia* frequencies in the neighborhood of 60-80%.

1
2
3 **Fig 6. Time to reach about 80% ($\pi/4$) coverage as a function of initial frequency in the**
4 **release area, p_0 .** The calculations assume $\rho p_0 = 0.2$. The small dots are produced with $\hat{p} = 0.2$;
5 the large dots with $\hat{p} = 0.3$. Green points are for Gaussian dispersal, blue points for Laplace, and
6 black for ExpSqrt.

7 **Robustness of coverage times to incomplete knowledge.** Although one can propose
8 optimal spacing and release areas for fixed ρ and p_0 , the optimal values are unlikely to be
9 achieved in practice because they depend critically on two parameters, the local dispersal
10 parameter σ and the value of the unstable equilibrium \hat{p} , that will be known only approximately.
11 Moreover, the geometry of field releases will be influenced by factors such as housing density
12 and type, barriers to wave movement, and local community acceptance. Although the fraction of
13 the target area in which releases are initially performed, ρ , is clearly under experimental control,
14 as is the initial frequency in those release areas, p_0 , it is important to understand the robustness of
15 the minimum times presented in Table 4 and Fig 6 to alternative release areas, R_I , which are
16 measured in units of σ .

17 Fig 7 summarizes the results for all three dispersal models, assuming that we initially
18 release over 20% of the target area ($\rho = 0.2$) and produce an initial infection frequency $p_0 = 0.8$
19 relatively rapidly. As R_I departs from the optima given in Table 4, Fig 7 shows how the time to
20 achieve 80% coverage increases relative to T_{opt} , the minimal time achievable. As expected from
21 Table 4, there is a fundamental asymmetry produced by the fact that the optimal R_I is typically
22 only about 25-30% larger than the minimal release size needed to produce an expanding wave.
23 Hence, undershooting the optimal release size by as little as 25% can lead to releases that
24 collapse rather than expand. In contrast, for a realistic range of unstable points and all three
25 models of dispersal, overshooting the optimal release area by 50% increases $T_{\pi/4}$ by less than
26 20%. Even releases twice as large as optimal increase $T_{\pi/4}$ by at most 43%. The clear implication

1 is that one should use conservatively large estimates of σ and \hat{p} to design releases that will
2 produce near-optimal results with little possibility of collapse. The practical implications of
3 Table 4 and Fig 6 are discussed below.

4
5 **Fig 7. Time to reach about 80% ($\pi/4$) coverage, relative to the minimum time, as a function**
6 **of release area.** For each model, release areas are measured relative to the release area, $R_{I(\text{opt})}$,
7 that produces T_{\min} for that model. The DTDS calculations assume Caspari-Watson dynamics with
8 $\rho = 0.2$ and $p_0 = 0.8$. The small dots are produced with $\hat{p} = 0.2$; the large dots with $\hat{p} = 0.3$.
9 Green points are for Gaussian dispersal, blue points for Laplace, and black for ExpSqrt.

10

11 **Discussion**

12 Early proposals by O’Neill and his collaborators (e.g., Sinkins et al. 1997) to transform natural
13 populations with introduced *Wolbachia* were motivated at least in part by the belief that even
14 fitness-decreasing infections might spread rapidly in nature, driven by the force of cytoplasmic
15 incompatibility (Turelli and Hoffmann 1991, 1995). However, the rapid spatial spread of natural
16 *Wolbachia* infections in *Drosophila* now seems dependent on net fitness advantages, previously
17 unknown – and still not fully understood, that allow them to increase systematically in frequency
18 even when they are so rare that cytoplasmic incompatibility provides no appreciable benefit
19 (Fenton et al. 2011; Kriesner et al. 2013; Hamm et al. 2014). For *Wolbachia* infections that tend
20 to increase when rare, occasional long-distance dispersal events can allow them to establish
21 locally, spread and coalesce with other propagules, speeding their spatial spread far beyond what
22 might be expected from more typical dispersal. Bistable dynamics, as produced by the
23 appreciable fitness costs associated with *wMel*-infected *Aedes aegypti* in Australia, restrict
24 spatial spread to speeds set by average dispersal. Moreover, bistability sets a fundamental
25 constraint on which transinfections might ever spread. S. L. O’Neill’s “Eliminate Dengue”
26 project (<http://www.eliminatedengue.com/program>) initially proposed introducing the life-

1 shortening *Wolbachia*, *wMelPop*, into *Ae. aegypti* to greatly reduce the frequency of females old
2 enough to transmit dengue virus. However, the fitness costs associated with *wMelPop* in *Ae.*
3 *aegypti* produced an unstable infection frequency far above 0.5, precluding spatial spread
4 (Barton 1979; Turelli 2010; Walker et al. 2011; Barton and Turelli 2011).

5

6 **Evidence for bistability**

7 Based on the theory in Barton and Turelli (2011) and the expectation that few mosquitoes
8 would cross the highway, Hoffmann et al. (2011) predicted that “Unless fitness costs are
9 essentially zero or there are unexpected fitness benefits, we do not expect the infection to spread
10 further ...” Four years later, *wMel* has not become established in PE despite repeated
11 immigration. An adaptation of Haldane’s (1930) island model (Eq. 1) indicates a lower bound on
12 the unstable equilibrium, \hat{p} , of about 0.21. This local frequency threshold for population
13 transformation appreciably slows the predicted rate of spatial spread, as indicated by Eq. 5.

14 Our new data and analyses bolster previous evidence for bistability. In Hoffmann et al.
15 (2011), an informal quantitative analysis of the rising frequency of *wMel* in response to several
16 weekly releases indicated fitness costs on the order of 20%. However, the frequency data could
17 not distinguish fitness costs associated with laboratory rearing from reduced fitness intrinsic to
18 the *Wolbachia* transinfection. Two years later, Hoffmann et al. (2014) resampled these stably
19 transformed populations and determined that the infected females produced about 20% fewer
20 eggs under laboratory conditions, suggesting that $\hat{p} \geq 0.2$. As a consequence of bistability, the
21 rate of spatial spread is limited by natural dispersal ability, with a maximum speed bounded
22 above by $\sigma/2$ per generation, where σ is the dispersal parameter discussed below. In particular,
23 bistability precludes very rapid spatial spread based on long-distance, human-mediated dispersal.
24 Even when large numbers are transported by accident, the area transformed would be unlikely to
25 exceed the minimum size needed to initiate spatial spread (Fig. 4).

26 The unstable equilibrium frequency, \hat{p} , is a useful abstraction that captures key features of
27 the complex frequency dynamics of *Wolbachia* transinfections. The true dynamics are

1 multidimensional (Turelli 2010; Zheng et al. 2014) and depend on age-specific effects as well as
2 ecological factors, such as intraspecific density-dependence (Hancock et al. 2011a,b; Hancock et
3 al. 2016) and interaction with other insects and microbes (Fenton et al. 2011). However, a full
4 description of this biology would involve many parameters that would have to be estimated in
5 each locale. We doubt that these parameters could be estimated accurately enough for more
6 realistic models to produce better predictions than our simple two-parameter approximations. Our
7 idealized models of frequency dynamics produce field-testable predictions and empirically useful
8 guidance for field releases.

9

10 **Predictions for spatial spread**

11 **Wave width.** The point of estimating wave width is that it provides an average estimate –
12 under natural field conditions – of the dispersal parameter σ that is central to predicting wave
13 speed (see Eqs. 5 and 6). Using discrete-time, discrete-space (DTDS) approximations with
14 alternative models of dispersal, we have tested the robustness of diffusion-based approximations
15 for wave speed, wave width and the size of releases needed to initiate spatial spread. The most
16 robust prediction concerns wave width (see Eq. 6 and Fig 3). For a wide range of dispersal
17 models and parameters, wave width is observed to be within about 10% of the analytical
18 prediction (Eq. 6) produced by the cubic-diffusion approximation for bistable dynamics. This
19 implies that estimates of the dispersal parameter σ can be obtained from data on the spatial
20 pattern of infection frequencies after local releases. Unlike dispersal estimates obtained from
21 short-term release-recapture experiments, estimates based on infection-frequency wave width
22 average over seasons and are largely free from behavioral artifacts associated with inflated
23 population densities or the effects of lab rearing, marking or handling.

24

25 **Wave speed.** The cubic-diffusion model produces the wave-speed approximation (Eq. 5): c
26 $= \sigma^{1/2} - \hat{p}$ per generation, assuming complete cytoplasmic incompatibility (i.e., $s_h = 1$ in Eq. 4a
27 or 8a). Our DTDS calculations show that this approximation remains accurate even for the rapid

1 local dynamics produced by complete CI if dispersal is near-Gaussian (i.e., Gaussian or Laplace
2 in Eq. 9) and the unstable point is below 0.4 (Fig 4B). However, for long-tailed dispersal as
3 described by the ExpSqrt model (see Eq. 9c and Fig 1), spatial spread is slowed by 30-40%
4 relative to the analytical prediction for $0.2 \leq \hat{p} \leq 0.35$. Hence, if σ is on the order of 100
5 m/(generation)^{1/2} and \hat{p} is near 0.25, the predicted wave speed can drop from about 25
6 m/generation to about 15 m/generation. The result is that with about 10 *Ae. aegypti* generations
7 per year, *wMel* is expected to spread through natural populations of *Ae. aegypti* at a rate nearly
8 three orders of magnitude slower than the 100 km/year rate at which *wRi* spread through *D.*
9 *simulans* populations in California and eastern Australia.

10

11 **Wave initiation.** Finally, our DTDS calculations indicate that the cubic-diffusion
12 approximations for the minimum radii of release areas from Barton and Turelli (2011) are likely
13 to be significant overestimates, especially if fitness is reduced primarily through fecundity. Fig 4
14 shows that the diffusion approximation may overestimate minimum release sizes by a factor of
15 two for $0.2 \leq \hat{p} \leq 0.35$. In general, for fixed σ , smaller releases will initiate spatial spread when
16 dispersal is more long-tailed. With $\sigma \approx 100$ m/(generation)^{1/2}, releases that produce initial
17 frequencies of 0.8 over about 0.13 km² should suffice to initiate spatial spread, assuming that \hat{p}
18 ≤ 0.3 . However, near this minimum, expansion (or collapse) is expected to be extremely slow,
19 easily on the order of two years.

20

21 **Predictions for Cairns releases**

22 In 2013, the *wMel* releases in the Edgehill/Whitfield (EHW) and Parramatta Park (PP) regions of
23 Cairns quickly produced infection frequencies about 0.8 within the release areas. Given that
24 these sites are roughly 0.97 km² (EHW) and 0.52 km² (PP), we expect spatial spread of the
25 infection from both release areas. Assuming $\sigma \approx 100$ m/(generation)^{1/2} (corresponding to wave
26 width on the order of 400 m), our analyses predict spread on the order of 10-25 m/generation,
27 assuming $\hat{p} \approx 0.25$. In contrast, the Westcourt (WC) release encompassed only 0.11 km², very

1 close to the critical value that separates expected local establishment from collapse, assuming \hat{p}
2 ≈ 0.25 and $100 \text{ m}/(\text{generation})^{1/2}$ (see Table 2 for additional details). Given the slow rate of
3 change expected near this threshold, considerable replication of such small releases would be
4 required to convert our ambiguous prediction into a rigorous test. In contrast to the difficulty of
5 testing our predictions concerning the minimum sizes of releases, our wave-speed and wave-
6 width predictions can be easily compared to empirical data from urban field releases. The
7 “Eliminate Dengue” project is currently preparing the data from the 2013 Cairns releases for
8 publication.

9

10 **Practical guidelines for field releases**

11 When the “Eliminate Dengue” program initially obtained Gates Foundation “Grand Challenges”
12 funding in 2006, the extraordinarily rapid spread of wRi through California populations of *D.*
13 *simulans* provided a plausible paradigm supporting the conjecture that natural *Ae. aegypti*
14 populations could be rapidly transformed with disease-suppressing *Wolbachia*. The *D. simulans*
15 paradigm also suggested that very few local introductions could lead to area-wide transformation
16 within a few years for large metropolitan areas with relatively continuous *Ae. aegypti* habitat.
17 Unfortunately, this rapid-spread paradigm, which remains demonstrably true for natural
18 *Wolbachia* infections (Kriesner et al. 2013), now seems clearly inapplicable to *Wolbachia*
19 transinfections that significantly reduce the fitness of their *Ae. aegypti* hosts. More plausible
20 rates of spatial spread seem to be at most 0.25 km per year, and even those slow rates are
21 expected only in near-continuous habitats. From our analysis of the Pyramid Estate data, it seems
22 that barriers on the order of 100-200 m, such as highways, will suffice to halt spread. Hence, it is
23 reasonable to ask whether spatial spread can play a significant role in achieving area-wide
24 coverage over a time scale of a few years.

25 A central question is whether real urban/suburban landscapes provide enough nearly-
26 continuous habitat to apply our optimal – or near-optimal – release designs, involving a series of
27 releases set out in grids. We have showcased an empirical example in which $wMel$ has

1 apparently not been able to cross a highway. We do not yet know enough to characterize a priori
2 the barriers that will halt wMel spread. What is clear is that area-wide control over just a few
3 years will require many release areas. We can offer simple guidance based on our mathematical
4 results and the population biology of vector-borne disease transmission. Given that spatial spread
5 will preferentially occur from high-density areas to low-density areas, a guiding principle is that
6 releases should initially occur in areas that support the highest *Ae. aegypti* densities. Because
7 disease transmission is proportional to vector density, these areas are the natural targets for initial
8 control efforts.

9 Our calculations provide more detailed guidance concerning the size of individual releases,
10 their spacing, and the initial infection frequencies that should be achieved. Fig 5 shows that for a
11 wide range of parameters, releases need not produce initial frequencies above 0.6. Indeed, the
12 effort to achieve much higher initial frequencies may produce slightly slower area-wide
13 coverage, if a fixed fraction of the local mosquito population is initially replaced. As
14 demonstrated by Fig 6, overshooting optimal release areas even by a factor of two should
15 increase the time to produce large-scale coverage by at most 50%. In contrast, Table 2 shows that
16 “optimal” release areas are often only twice as large as the minimal release areas needed to
17 initiate spread (corresponding to $R_1/R_{crit} = \sqrt{2}$ in Table 2). Thus, release areas should be based on
18 conservatively large estimates of σ and \hat{p} . Assuming $\sigma \leq 120$ m/gen^{1/2} and $\hat{p} \leq 0.3$, individual
19 releases on the order of 1 km², producing initial frequencies of 60-80%, should generally suffice
20 to guarantee local spread, assuming that the surrounding habitat has population densities
21 comparable to or lower than the release area. If the habitat is sufficiently homogeneous, covering
22 only about a third of the target area with such releases should produce about 80% coverage in
23 less than three years.

24 All of our guidelines are predicated on $\hat{p} \leq 0.35$. The lower the unstable point the better.
25 But if there is any significant cost of *Wolbachia* transinfections, so that $\hat{p} \geq 0.1$, wave speed is
26 likely to be bounded above by $\sigma/2$. Although spatial spread of low- \hat{p} variants is unlikely to be
27 significantly aided by occasional long-distance dispersal, the spread of such variants is far less

1 likely to be stopped by minor barriers to dispersal. As shown in Fig 6 of Barton and Turelli
2 (2011), step-increases in population density of just over two-fold will stop the spatial spread of a
3 transinfection that produces $\hat{p} = 0.25$; whereas an increase greater than five-fold is needed to
4 stop a variant with $\hat{p} = 0.1$.

5 Given that only two *Wolbachia* transfections of *Ae. aegypti* have been released in nature in
6 population transformation efforts, we don't know whether there are *Wolbachia* variants that can
7 provide effective virus-blocking and produce low fitness costs. In preliminary analyses, high
8 *Wolbachia* titer is associated with better virus blocking and also lower fitness of infected hosts
9 (Walker et al. 2011; Martinez et al. 2015). Among *Wolbachia* found in *Drosophila* species and
10 transferred into *D. simulans*, the relationships between titer and measures of fitness loss and
11 virus protection are both highly significant; but they explain only about half of the variation
12 observed in each trait. Hence, it seems likely that further exploration of *Wolbachia* variation in
13 nature could uncover high-protection, low-fitness-cost variants.

14 Despite the fact that the *wMel* variant currently being released will spread very slowly and
15 may be relatively easily stopped by barriers to dispersal, it still offers significant benefits over
16 disease-control strategies like insecticide application and sterile-male release (or release of CI-
17 causing males) that require continual applications to suppress local vector populations (McGraw
18 and O'Neill 2013). As shown by Hoffmann et al. (2014), transformations of isolated populations
19 with *Wolbachia* remain stable. Similarly, for sufficiently large local releases, we expect local
20 *Wolbachia* introductions to at least persist and probably slowly expand as long as the
21 surrounding areas do not harbor significantly higher *Ae. aegypti* densities. Even if half of a large
22 area has to be actively transformed to achieve area-wide control, this will only have to be done
23 once. We do not know how long-lasting dengue-blocking by *wMel* or other transinfections will
24 be, but the comparative evidence from natural *Wolbachia* infections suggests that it should
25 persist for at least a decade or more (Bull and Turelli 2013), a time-scale over which effective
26 vaccines may well become available (Screaton et al. 2015).

27

1 **References**

- 2 Barton NH. Dynamics of hybrid zones. *Heredity* 1979;43:341–359.
- 3 Barton NH, Hewitt GM. Analysis of hybrid zones. *Annu Rev Ecol Syst* 1985;16:113–148.
- 4 Barton NH, Turelli M. Spatial waves of advance with bistable dynamics: cytoplasmic and
5 genetic analogues of allee effects. *Am Nat* 2011;178:E48–E75.
- 6 Bian G, Joshi D, Dong Y, Xie Y, Xi, Z. *Wolbachia* invades *Anopheles stephensi* populations and
7 induces refractoriness to *Plasmodium* infection. *Science* 2013;340:748–751.
- 8 Brown JE, McBride CS, Johnson P, Ritchie S, Paupy C, Bossin H, et al. Worldwide patterns of
9 genetic differentiation imply multiple domestications of *Aedes aegypti*, a major vector of
10 human diseases. *Proc R Soc Lond B Biol Sci* 2011;278:2446–2454.
- 11 Brownlie JC, Cass BN, Riegler M, Witsenburg JJ, Iturbe-Ormaetxe I, McGraw EA, et al.
12 Evidence for metabolic provisioning by a common endosymbiont, *Wolbachia pipientis*,
13 during periods of nutritional stress. *PLoS Pathog* 2009;5:e1000368.
- 14 Bull JJ, Turelli M. *Wolbachia* versus dengue: evolutionary forecasts. *Evol Med Public Health*
15 2013:197–207.
- 16 Carrington LB, Lipkowitz JR, Hoffmann AA, Turelli M. A re-examination of *Wolbachia*-
17 induced cytoplasmic incompatibility in California *Drosophila simulans*. *PloS One*
18 2011;6:e22565
- 19 Caspari E, Watson GS. On the evolutionary importance of cytoplasmic sterility in mosquitoes.
20 *Evolution* 1959;13:568–570.
- 21 Coyne JA, Boussy IA, Prout T, Bryant SH, Jones JS, Moore JA. Long-distance migration of
22 *Drosophila*. *Am Nat* 1982;119:589–595.
- 23 Coyne JA, Bryant SH, Turelli M. Long-distance migration of *Drosophila*. 2. Presence in desolate
24 sites and dispersal near a dessert oasis. *Am Nat* 1987;126:847–861.
- 25 Dobzhansky Th, Wright S. Genetics of natural populations. X. Dispersion rates in *Drosophila*

- 1 *pseudoobscura*. *Genetics* 1943;28:304–340.
- 2 Dodson BL, Hughes GL, Paul O, Matacchiero AC, Kramer LD, Rasgon JL. *Wolbachia* enhances
3 West Nile virus (WNV) infection in the mosquito *Culex tarsalis*. *PLoS Negl Trop Dis*
4 2014;8:e2965.
- 5 Dutra HLC, Rocha MN, Dias FBS, Mansur SB, Caragata EP, Moreira LA. *Wolbachia* blocks
6 currently circulating Zika virus isolates in Brazilian *Aedes aegypti* mosquitos. *Cell Host &*
7 *Microbe* 2016;19:1–4.
- 8 Endler JA. *Geographic variation, speciation, and clines*. Princeton: Princeton University Press;
9 1977.
- 10 Fenton A, Johnson KN, Brownlie JC, Hurst GDD. Solving the *Wolbachia* paradox: modeling the
11 tripartite interaction between host, *Wolbachia*, and a natural enemy. *Am Nat* 2011;178:333–
12 342.
- 13 Ferguson NM, Kien DTH, Clapham H, Aguas R, Trung VT, Chau TNB, et al. Modeling the
14 impact on virus transmission of *Wolbachia*-mediated blocking of dengue virus infection of
15 *Aedes aegypti*. *Sci Transl Med* 2015;7:279ra37.
- 16 Frentiu FD, Zakir T, Walker T, Popovici J, Pyke AT, van den Hurk A, et al. Limited dengue
17 virus replication in field-collected *Aedes aegypti* mosquitoes infected with *Wolbachia*. *PLoS*
18 *Negl Trop Dis* 2014;8:e2688.
- 19 Gill AC Darby AC, Makepeace BL. Iron necessity: The secret of *Wolbachia*'s success? *PLoS*
20 *Negl Trop Dis* 2014;8:e3224.
- 21 Haldane JBS. A mathematical theory of natural and artificial selection. Part VI. Isolation.
22 *Proceedings of the Cambridge Philosophical Society* 1930;26:220–230
- 23 Haldane JBS. The theory of a cline. *J Genet* 1948;48:277–283.
- 24 Hamm CA, Begun DJ, Vo A, Smith CCR, Saelao P, Shaver AO, et al. *Wolbachia* do not live by
25 reproductive manipulation alone: infection polymorphism in *Drosophila suzukii* and *D.*

- 1 *subpulchrella*. Mol Ecol 2014;23:4871–4885.
- 2 Hancock PA, Sinkins SP, Godfray HCJ. Population dynamic models of the spread of *Wolbachia*.
3 Am Nat 2011a;117:323–333.
- 4 Hancock PA, Sinkins SP, Godfray HCJ. Strategies for introducing *Wolbachia* to reduce
5 transmission of mosquito-borne diseases. PLoS Negl Trop Dis 2011b;5:e1024.
- 6 Hancock PA, Linley-White V, Callahan AG, Godfray HCJ, Hoffmann AA, Ritchie SA. Density-
7 dependent population dynamics in *Aedes aegypti* slow the spread of *wMel Wolbachia*. J Appl
8 Ecol 2016;in press.
- 9 Harcombe W, Hoffmann AA. *Wolbachia* effects in *Drosophila melanogaster*: in search of fitness
10 benefits. J Invertebr Pathol 2004;87:45–50.
- 11 Harrington LC, Scott TW, Lerdthusnee K, Coleman RC, Costero A, Clark GC, et al. Dispersal of
12 the dengue vector *Aedes aegypti* within and between rural communities. Am J Trop Med Hyg
13 2005;72:209–220.
- 14 Haygood R, Turelli M. Evolution of incompatibility-inducing microbes in subdivided host
15 populations. Evolution 2009;63:432–447.
- 16 Hedges LM, Brownlie JC, O'Neill SL, Johnson KN. *Wolbachia* and virus protection in insects.
17 Science 2008;322:702.
- 18 Hemme RR, Thomas CL, Chadee DD, Severson DW. Influence of urban landscapes on
19 population dynamics in a short-distance migrant mosquito: evidence for the dengue vector
20 *Aedes aegypti*. PLoS Negl Trop Dis 2010;4:e634.
- 21 Hoffmann AA. Partial incompatibility between two Australian populations of *Drosophila*
22 *melanogaster*. Entomol Exp Appl 1988;48:61–67.
- 23 Hoffmann AA, Turelli M. Unidirectional incompatibility in *Drosophila simulans*: Inheritance,
24 geographic variation and fitness effects. Genetics 1988;119:435–444.
- 25 Hoffmann AA, Turelli M. Cytoplasmic incompatibility in insects. In: O'Neill SL, Hoffmann AA,

- 1 Werren JH, editors. Influential Passengers: Inherited Microorganisms and Arthropod
2 Reproduction. New York: Oxford University Press; 1997. p. 42–80.
- 3 Hoffmann AA, Clancy D, Duncan J. Naturally-occurring *Wolbachia* infection in *Drosophila*
4 *simulans* that does not cause cytoplasmic incompatibility. *Heredity* 1996;76:1–8.
- 5 Hoffmann AA, Hercus M, Daghar H. Population dynamics of the *Wolbachia* infection causing
6 cytoplasmic incompatibility in *Drosophila melanogaster*. *Genetics* 1998;148:221–231.
- 7 Hoffmann AA, Montgomery BL, Popovici J, Iturbe-Ormaetxe I, Johnson PH, Muzzi F, et al.
8 Successful establishment of *Wolbachia* in *Aedes* populations to suppress dengue transmission.
9 *Nature* 2011;476:454-457.
- 10 Hoffmann AA, Turelli M, Harshman LG. Factors affecting the distribution of cytoplasmic
11 incompatibility in *Drosophila simulans*. *Genetics* 1990;126:933–948.
- 12 Hoffmann AA, Iturbe-Ormaetxe I, Callahan AG, Phillips BL, Billington K, Axford JK, et al.
13 Stability of the *wMel* *Wolbachia* infection following invasion into *Aedes aegypti* populations.
14 *PLoS Negl Trop Dis* 2014;8:e3115.
- 15 Jansen VAA, M Turelli M, Godfray HCJ. Stochastic spread of *Wolbachia*. *Proc R Soc Lond B*
16 *Biol Sci* 2008;275:2769-2776.
- 17 Kriesner P, Hoffmann AA, Lee SF, Turelli M, Weeks AR. Rapid sequential spread of two
18 *Wolbachia* variants in *Drosophila simulans*. *PLoS Pathog* 2013;9:e1003607.
- 19 Laven H. Eradication of *Culex pipiens fatigans* through cytoplasmic incompatibility. *Nature*
20 1967;216:383–384.
- 21 Martinez J, Longdon B, Bauer S, Chan Y-S, Miller WJ, Bourtzis K, et al. Symbionts commonly
22 provide broad spectrum resistance to viruses in insects: a comparative analysis of *Wolbachia*
23 strains. *PLoS Pathog* 2014;10:e1004369.
- 24 Martinez J, Ok S, Smith S, Snoeck K, Day JP, Jiggins FM. Should symbionts be nice or selfish?
25 Antiviral effects of *Wolbachia* are costly but reproductive parasitism is not. *PLoS Pathog*

- 1 2015;10:e1005021.
- 2 McGraw EA, O'Neill SL. Beyond insecticides: new thinking on an ancient problem. *Nat Rev*
3 *Microbiol* 2013;11:181–193.
- 4 McInnis DO, Schaffer HE, Mettler LE. Field dispersal and population sizes of native *Drosophila*
5 from North Carolina. *Am Nat* 1982;119:319–330.
- 6 McMeniman CJ, Lane RV, Cass BN, Fong AWC, Sidhu M, Wang Y-F, et al. Stable introduction
7 of a life-shortening *Wolbachia* infection into the mosquito *Aedes aegypti*. *Science*
8 2009;323:141–144.
- 9 Nagylaki T. Conditions for the existence of clines. *Genetics* 1975;80: 595-615.
- 10 Nigro L, Prout T. Is there selection on RFLP differences in mitochondrial DNA? *Genetics*
11 1990;125:551–555.
- 12 Osborne SE, Leong YS, O'Neill SL, Johnson KN. Variation in antiviral protection mediated by
13 different *Wolbachia* strains in *Drosophila simulans*. *PLoS Pathog* 2009;5:e1000656.
- 14 Powell JR, Dobzhansky Th, Hook JE, Wistrand HE. *Genetics of natural populations. XLIII.*
15 Further studies on rates of dispersal of *Drosophila pseudoobscura* and its relatives. *Genetics*
16 1976;82:493–506.
- 17 Prout T. Some relationships between density-independent selection and density-dependent
18 population growth. *Evol Biol* 1980;13:1–68.
- 19 Reynolds KT, Hoffmann AA. Male age, host effects and the weak expression or non-expression
20 of cytoplasmic incompatibility in *Drosophila* strains infected with maternally transmitted
21 *Wolbachia*. *Genet Res* 2002;80:79–87.
- 22 Richardson MF, Weinert LA, Welch JJ, Linheiro RS, Magwire MM, Jiggins FM, et al.
23 Population genomics of the *Wolbachia* endosymbiont in *Drosophila melanogaster*. *PLoS*
24 *Genet* 2012;8:e1003129.
- 25 Riegler M, Sidhu M, Miller MJ, O'Neill SL. Evidence for a global *Wolbachia* replacement in

- 1 *Drosophila melanogaster*. *Curr Biol* 2005;15:1428–1433.
- 2 Ritchie SA, Montgomery BL, Hoffmann AA. Novel estimates of *Aedes aegypti* (Diptera:
3 Culicidae) population size and adult survival based on *Wolbachia* releases. *J Med Entomol*
4 2013;50:624–631.
- 5 Russell RC, Webb CE, William CR, Ritchie SA. Mark-release-recapture study to measure
6 dispersal of the mosquito *Aedes aegypti* in Cairns, Queensland, Australia. *Med Vet Entomol*
7 2005;19:451–457.
- 8 Schraiber J, Silverstein R, Kaczmarczyk AN, Kwok R, Park M, Rutaganira T et al. Constraints
9 on the use of lifespan-shortening *Wolbachia* to control dengue fever. *J Theor Biol*
10 2012;297:26–32.
- 11 Screaton G, Mongkolsapaya J, Yacoub S, Roberts C. New insights into the immunopathology
12 and control of dengue virus infection. *Nat Rev Immunol* 2015;15:745–759.
- 13 Shigesada N, Kawasaki K. *Biological invasions: theory and practice*. Oxford: Oxford University
14 Press; 1997.
- 15 Sinkins SP, Curtis CF, O’Neill SL. The potential application of inherited symbiont systems to
16 pest control. In: O’Neill SL, Hoffmann AA, Werren JH, editors. *Influential Passengers:*
17 *Inherited Microorganisms and Arthropod Reproduction*. New York: Oxford University Press;
18 1997. p. 42–80.
- 19 Slatkin M. Gene flow and selection in a cline. *Genetics* 1973;75:733–756.
- 20 Teixeira L, Ferreira A, Ashburner M. The bacterial symbiont *Wolbachia* induces resistance to
21 RNA viral infections in *Drosophila melanogaster*. *Plos Biol* 2008;6:e1000002.
- 22 Turelli M. Evolution of incompatibility-inducing microbes and their hosts. *Evolution*
23 1994;48:1500–1513.
- 24 Turelli M. Cytoplasmic incompatibility in populations with overlapping generations. *Evolution*
25 2010;64:232–241.

- 1 Turelli M, Hoffmann AA. Rapid spread of an inherited incompatibility factor in California
2 *Drosophila*. *Nature* 1991;353:440–442.
- 3 Turelli M, Hoffmann AA. Cytoplasmic incompatibility in *Drosophila simulans*: dynamics and
4 parameter estimates from natural populations. *Genetics* 1995;140:1319–1338.
- 5 Walker T, Johnson PH, Moreira LA, Iturbe-Ormaetxe I, Frentiu FD, McMeniman CJ, et al. The
6 *wMel* *Wolbachia* strain blocks dengue and invades caged *Aedes aegypti* populations. *Nature*
7 2011;476:450–453.
- 8 Walsh RK, Aguilar CL, Facchinelli L, Valerio L, Ramsey JM, Scott TW, et al. Regulation of
9 *Aedes aegypti* population dynamics in field systems: quantifying direct and delayed density
10 dependence. *Am J Trop Med Hyg* 2013;89:68–77.
- 11 Wang M-H, Kot M, Neubert MG. Integro-difference equations, Allee effects, and invasions. *J*
12 *Math Biol* 2002;44:150–168.
- 13 Weeks AR, Turelli M, Harcombe WR, Reynolds KT, Hoffmann AA. From parasite to mutualist:
14 rapid evolution of *Wolbachia* in natural populations of *Drosophila*. *PLoS Biol* 2007;5:997–
15 1005.
- 16 Weinert LA, Araujo-Jnr EV, Ahmed MZ, Welch JJ. The incidence of bacterial endosymbionts in
17 terrestrial arthropods. *Proc R Soc Lond B Biol Sci* 2015;282:20150249.
- 18 Werren JH, Baldo L, Clark ME. *Wolbachia*: master manipulators of invertebrate biology. *Nat*
19 *Rev Microbiol* 2008;6:741–751.
- 20 Zheng B, Tang M, Yu J. Modeling *Wolbachia* spread in mosquitoes through delay differential
21 equations. *SIAM J Appl Math* 2014;74:743–770.

22

23 **Supporting Information**

24 **S1 File. Appendix A.** Effect of dispersal pattern and random fluctuations on travelling waves.

25 **S2 File. Appendix B.** Establishing a wave.

Acknowledgments

We thank A. A. Hoffmann and S. L. O'Neill and three reviewers for constructive comments on earlier drafts. This work was supported in part by grants from the Joel Keizer Endowment to UC Davis (MT), the Foundation for the National Institutes of Health through the Grand Challenges in Global Health Initiative of the Bill and Melinda Gates Foundation (MT), and National Institutes of Health grant R01-GM-104325-01 (MT).

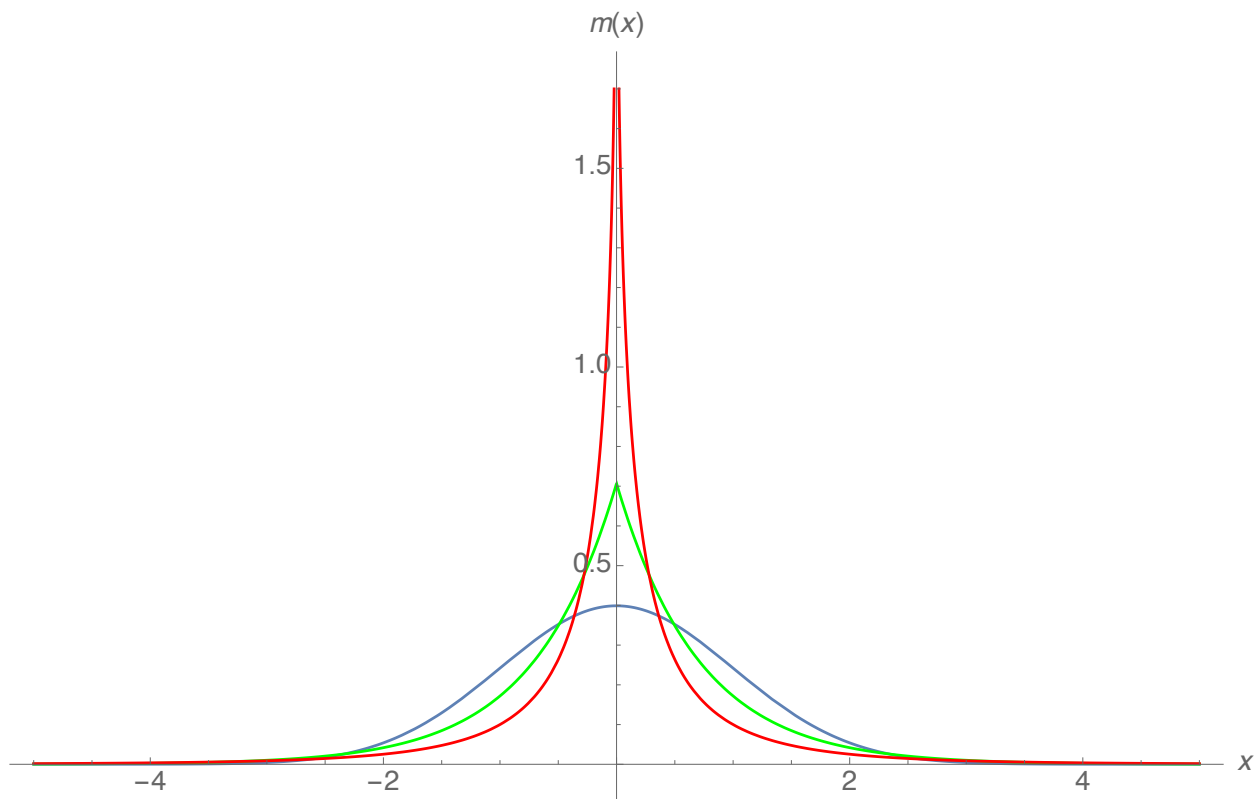


Fig 1. Alternative dispersal models with $\sigma = 1$. The three models are: Gaussian (blue), Laplace (green), and ExpSqrt (red) as described by (9). Each describes the probability, denoted $m(x)$ in the figure, of moving distance x along any axis.

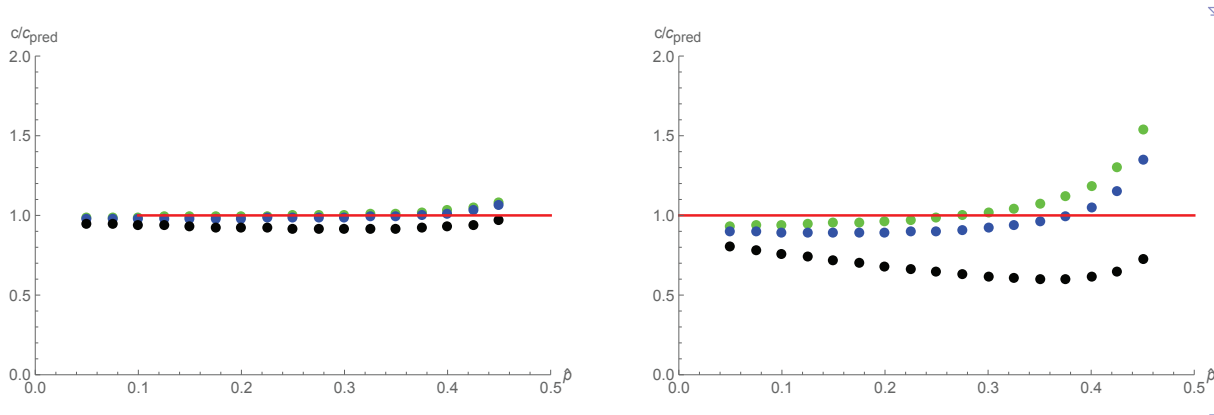


Fig 2. Wave speed. Speed calculated from DSDT analyses compared to the cubic-based diffusion prediction, $c = \sigma\sqrt{s_h}(\frac{1}{2} - \hat{\rho})$, as a function of $\hat{\rho}$, for $s_h = 0.2$ (left) and $s_h = 1$ (right). The green dots were produced with Gaussian dispersal, blue with Laplace and black with Exponential Square root (ExpSqrt).

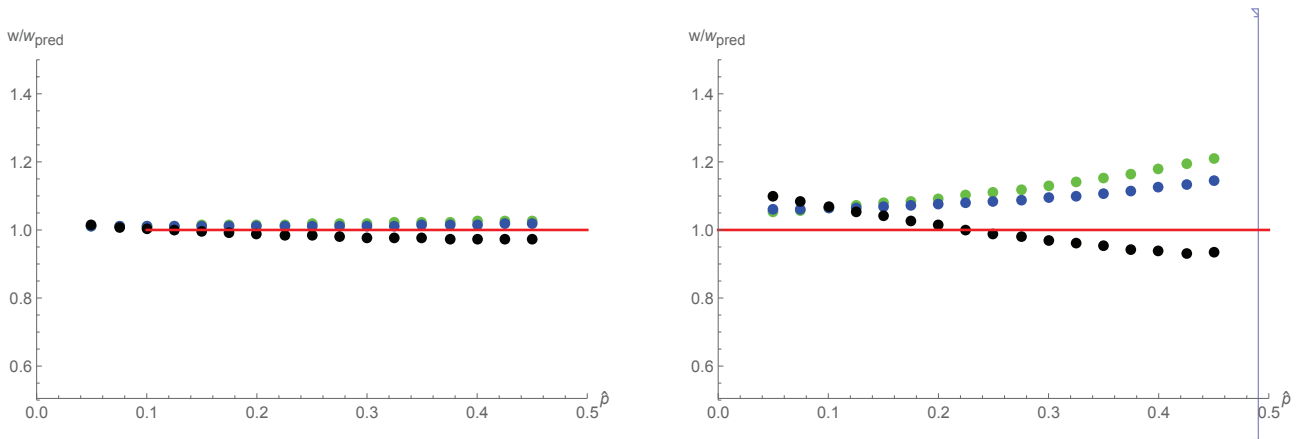


Fig 3. Wave width. Wave width as a function of \hat{p} calculated using discrete-time, discrete-space (DTDS) analyses with alternative dispersal models. The dots from the DTDS analyses are compared to the diffusion prediction ($w = 1/\text{Max}(|\partial p/\partial x|) = 4\sigma/\sqrt{s_h}$, red line) for $s_h = 0.2$ (left) and $s_h = 1$ (right). The green dots were produced with Gaussian dispersal, blue with Laplace and black with Exponential Square root (ExpSqrt).

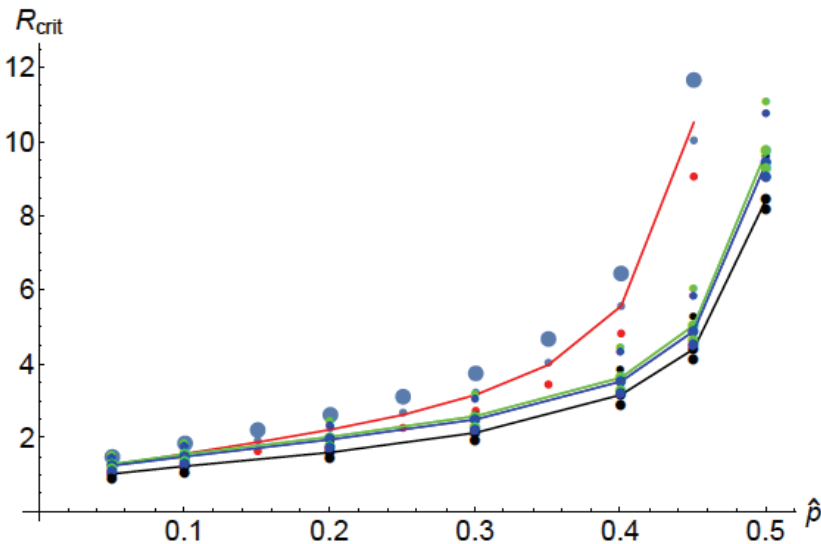


Fig 4. Critical radius, R_{crit} , assuming complete CI and Caspari-Watson dynamics. The upper points reproduce the diffusion results from Barton and Turelli (2011) with cubic (red curve) and Schraiber et al. (2012) CI dynamics. The red curve shows the cubic-diffusion predictions with $p_0 = 0.8$, the large blue dots are the cubic with $p_0 = 0.6$. The small red (blue) dots are produced by the diffusion analysis of Schraiber et al. (2012) CI dynamics with $p_0 = 0.8$ ($p_0 = 0.6$), assuming only viability fitness costs. The lower points and curves show our DTDS predictions as a function of \hat{p} and the initial infection frequency (p_0) with alternative dispersal models. The lower lines correspond to $p_0 = 0.8$ with Gaussian (green), Laplace (blue) and ExpSqrt (black) dispersal. The points above and below these lines correspond to $p_0 = 0.6$ and $p_0 = 1$, respectively.

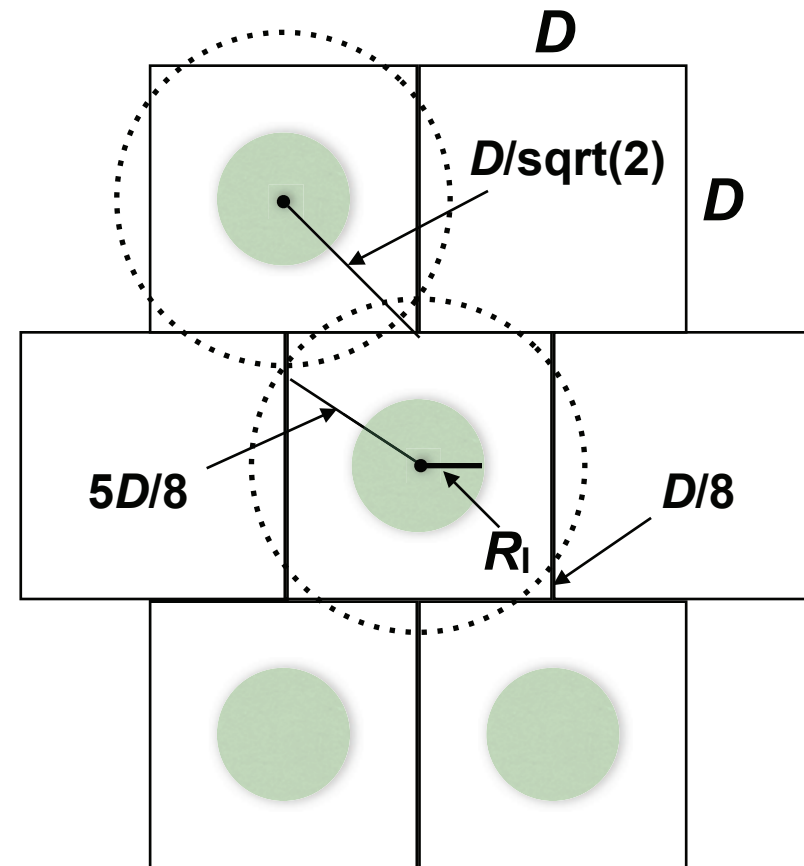


Fig 5. Optimal spacing. The green circles within the $D \times D$ squares represent release areas with radii R_1 . If the release areas were laid out on a regular grid, each expanding wave would have to travel to the corner of the enclosing square, a distance of $\sqrt{2}D - R_1$, to transform the entire target area. In contrast, by offsetting the release centers between adjacent rows, as illustrated, each wave must travel only $5D/8 - R_1$ for area-wide transformation.

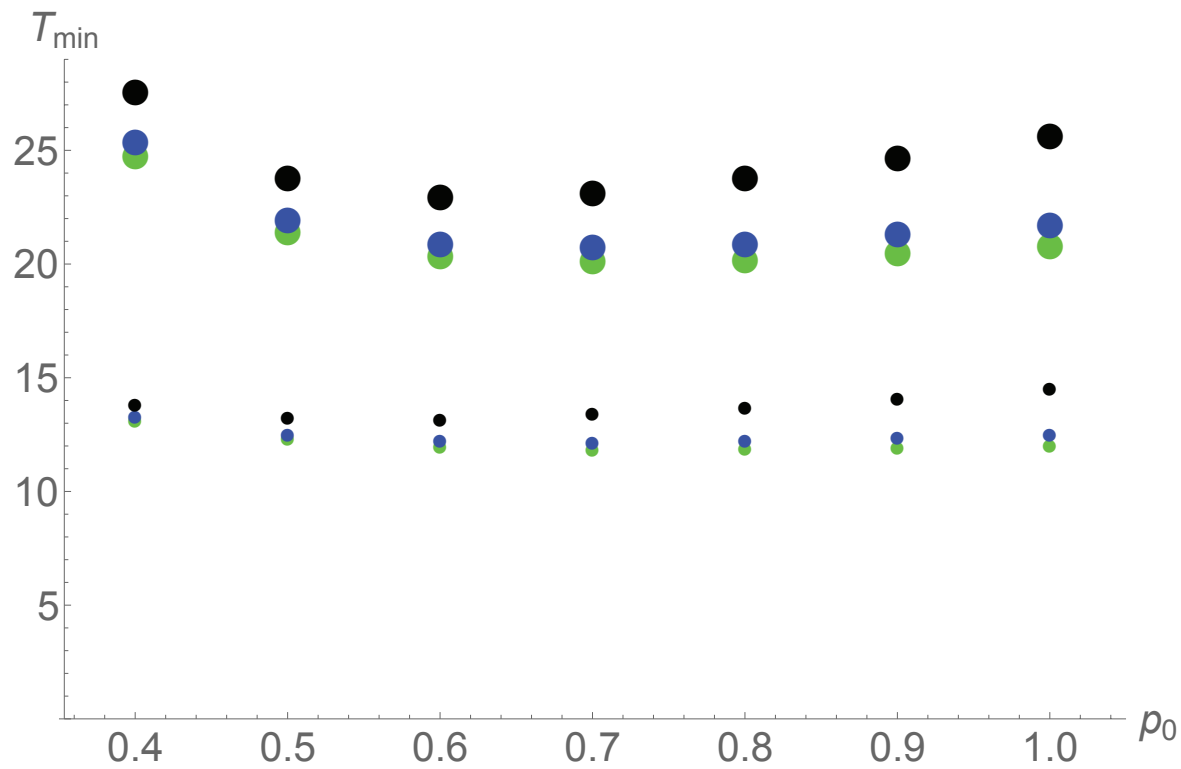


Fig 6. Time to reach about 80% ($\pi/4$) coverage as a function of initial frequency in the release area, p_0 . The calculations assume $\rho p_0 = 0.2$. The small dots are produced with $\hat{p} = 0.2$; the large dots with $\hat{p} = 0.3$. Green points are for Gaussian dispersal, blue points for Laplace, and black for ExpSqrt.

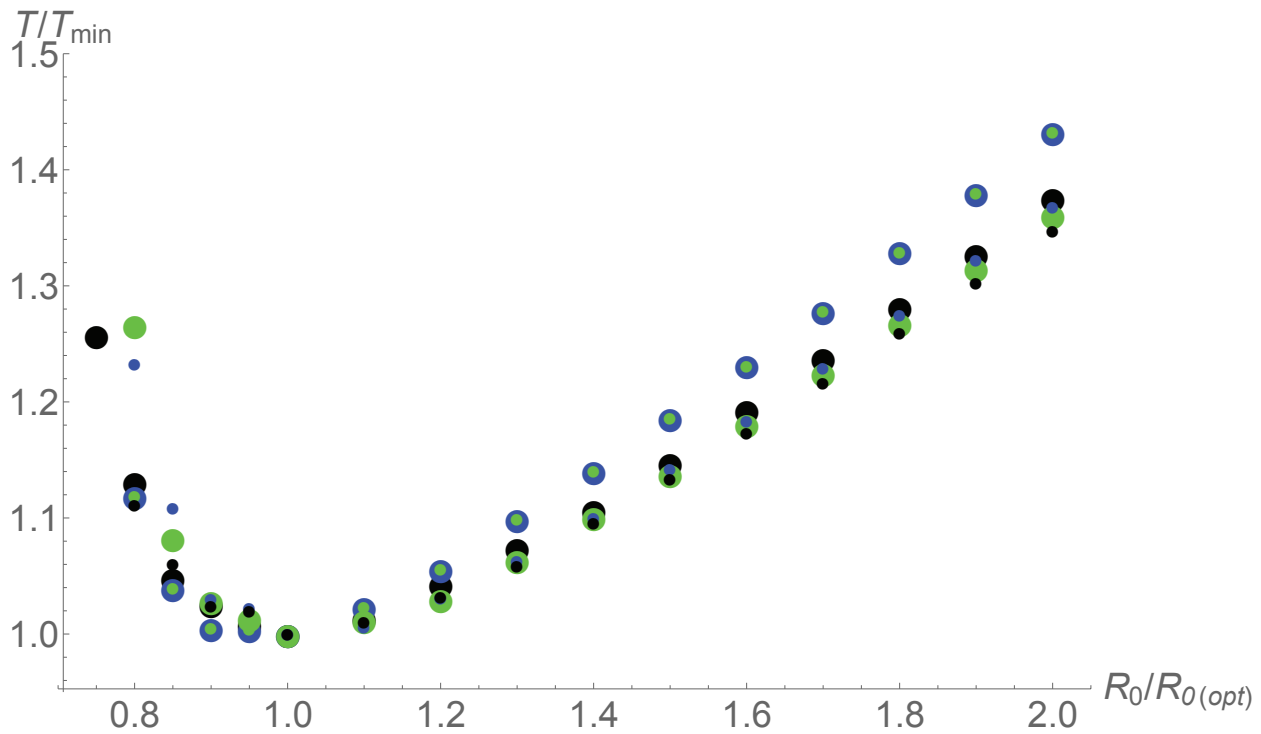


Fig 7. Time to reach about 80% ($\pi/4$) coverage, relative to the minimum time, as a function of release area. For each model, release areas are measured relative to the release area, $R_{I(opt)}$, that produces T_{\min} for that model. The DTDS calculations assume Caspari-Watson dynamics with $\rho = 0.2$ and $p_0 = 0.8$. The small dots are produced with $\hat{p} = 0.2$; the large dots with $\hat{p} = 0.3$. Green points are for Gaussian dispersal, blue points for Laplace, and black for ExpSqrt.

Appendix A: Effect of dispersal pattern and random fluctuations on travelling waves

Ultimately, populations consist of reproducing individuals. In continuous space, they may be approximated by deterministic integro-difference equations (IDE; Wang et al. 2002) in which allele frequencies or species density is taken to be continuous through space:

$$p_t[\mathbf{x}] = \int \phi[\mathbf{x}, \mathbf{y}] g[p_{t-1}[\mathbf{y}]] d\mathbf{y} \quad (1)$$

where $\phi[\mathbf{x}, \mathbf{y}]$ is the probability of moving from \mathbf{y} to \mathbf{x} . If change is sufficiently slow, and dispersal local, then this may be further approximated by a spatial diffusion, continuous in time, t , as well as space, \mathbf{x} :

$$\partial_t p = \frac{\sigma^2}{2} \frac{\partial^2 p}{\partial \mathbf{x}^2} + f[p] \quad (2)$$

where $f[p] = g[p] - p$, and $\sigma^2 = \int \phi[\epsilon] \epsilon^2 d\epsilon$ is the variance of dispersal distance. In the following numerical examples, we divide the habitat into discrete demes, and simulate a discrete stepping-stone model. However, we choose a large enough dispersal range that the deme spacing has negligible effect.

Under the diffusion approximation, the direction of movement is determined by whether the net rate of increase, $\int_0^1 f[p] dp$, is positive or negative. This simple result carries over to IDE models, and is independent of the form of dispersal, ϕ , provided that dispersal is symmetric. In stochastic models, the extent of spread (as measured by $\int p dx$, say) varies randomly, but the expected rate of spread still follows the same rule.

There is a qualitative distinction between two kinds of wave: *pushed* versus *pulled* (Stokes 1976). If $f[p] \geq pf'[0]$ for some $0 < p < 1$, then there will be a travelling wave that is pushed by increase within its bulk, and so which is insensitive to long-range dispersal, or to random fluctuations. With random sampling drift or demographic stochasticity, the variance in position increases by $\sim \frac{1}{N}$ in one dimension, where population density is N . In contrast, if $f < pf'[0]$ everywhere, then the wave is pulled at a rate determined by the individuals at the advancing front; individuals behind the wave almost all descend from this small fraction (Brunet et al. 2006). Now, the spread of the wave is sensitive to the form of long-range dispersal, and to the population density. Provided that the dispersal distribution is bounded by an exponential, the wave will settle to a steady shape, with a speed that depends only on the growth rate from low density; random fluctuations will slow it by an amount that depends logarithmically on density (Brunet et al. 2006). If the rate of long-range dispersal is faster than exponential, then the wave will accelerate, though again, random fluctuation will limit this acceleration, and cause the wave to fragment.

Effect of dispersal distribution on wave speed: deterministic models

We illustrate these points using the simple cubic model:

$$f[p] = \frac{s}{2} pq(p - q + \alpha) = spq(p - \hat{p}) \quad (3)$$

where $p + q = 1$. Note that the model only makes sense for sufficiently small s : it can be taken as a weak-selection approximation to a variety of more detailed models (Barton and Turelli, 2011). However, it is accurate even for quite large s , and so we take it as a surrogate for a much wider class of models.

Because we will be considering the case $\hat{p} < 0$, it is more natural to use the parameter α in this section.

Without loss of generality, we assume $\hat{p} < \frac{1}{2}$, or $\alpha = 1 - 2\hat{p} > 0$. If $\hat{p} > 0$, $\alpha < 1$, there is an unstable

equilibrium, whereas if $\hat{p} < 0$, $\alpha > 1$, the allele can increase from low frequency. ($\hat{p} = 0$ represents selection on a strictly recessive allele). If $\alpha < 3$ or $\hat{p} > -1$, then $f[p] \geq pf'[0]$ for some p , and so a pushed wave solution exists. However, a pulled solution also exists, with speed $c = \sigma \alpha \sqrt{s/4}$. The transition between a pulled and pushed wave occurs when the speeds of the two solutions intersect, at $\alpha = 2$, or $\hat{p} = -\frac{1}{2}$. For larger α , the deterministic solution is "pulled", with speed $c = \sigma \sqrt{s(\alpha - 1)} = \sigma \sqrt{2s(-\hat{p})}$ (Fisher 1937).

Figure 1 shows how the wave speed increases with α , measured relative to the prediction for a pushed wave, $\alpha \sigma \sqrt{s/4}$ (horizontal line). For Gaussian dispersal, the speed is very close to the diffusion approximation for $\alpha < 2$, and close to the prediction for a pulled wave, $c = \sigma \sqrt{s(\alpha - 1)}$, for $\alpha > 2$ (see below). A reflected exponential ("Laplace") distribution, which has substantially fatter tails, is also close to the diffusion approximation for a pulled wave (blue dots to right), but is slightly slower than predicted for a pushed wave for $\alpha < 1$. This is because genes that move a long way will be at a selective disadvantage, and so will be lost: the wave speed depends on the shape of the bulk of the dispersal kernel, which for a given variance, is narrower than a Gaussian (Fig. 2). The exponential square root distribution has even fatter tails, and shows a correspondingly slower speed for $\alpha < 1$. For $\alpha \geq 2$, this fat-tailed distribution gives a higher speed, but still settles to a travelling wave with constant speed. This is at first puzzling, since distributions with fatter than exponential tails are predicted to give an accelerating wave. However, numerical calculations were made with a dispersal distribution truncated at ± 20 demes, or ± 10 standard deviations (black dots). If this truncation is increased to 50 or 100 demes (purple and red dots), this makes little difference to the wave speed for $\alpha < 1$ (speeds are indistinguishable for $\alpha < 1$), but substantially increases the speed for $\alpha > 1$, as predicted. However, the speed is only increased by $\sim 20\%$ even when individuals can disperse out to 100 demes, or $\pm 50\sigma$. Moreover, even for the exponential square root distribution, only an extremely small fraction of the distribution is excluded by truncation at 25σ . Arguably, it would be unrealistic to calculate for yet longer tails, since real ranges are finite, and since over such large distances, stochastic effects will dominate even in very large populations, as we discuss below.

Figure 1. Wave speed, c , relative to that expected for a pushed wave, $\alpha \sigma \sqrt{s/4}$, is plotted against $\alpha = 1 - 2\hat{p}$. The horizontal line at 1 is the expectation for a pushed wave, whilst the downward curve at the right is the ratio expected for a pulled wave, whose speed is $c = \sigma \sqrt{s(\alpha - 1)}$. Dots show numerical calculations for three forms of dispersal: Gaussian (green), Laplace (blue), and exponential square root (black); the dispersal distribution is truncated at ± 20 demes, and the standard deviation adjusted to equal $\sigma = 2$. For the exponential square root, results are also shown for truncation at ± 50 demes (purple) and ± 100 demes (red). The selection coefficient is adjusted so that the maximum rate of change is always 0.025; this is equivalent to constant directional selection of $s = 20\%$. With these parameters, the deme spacing has negligible effect.

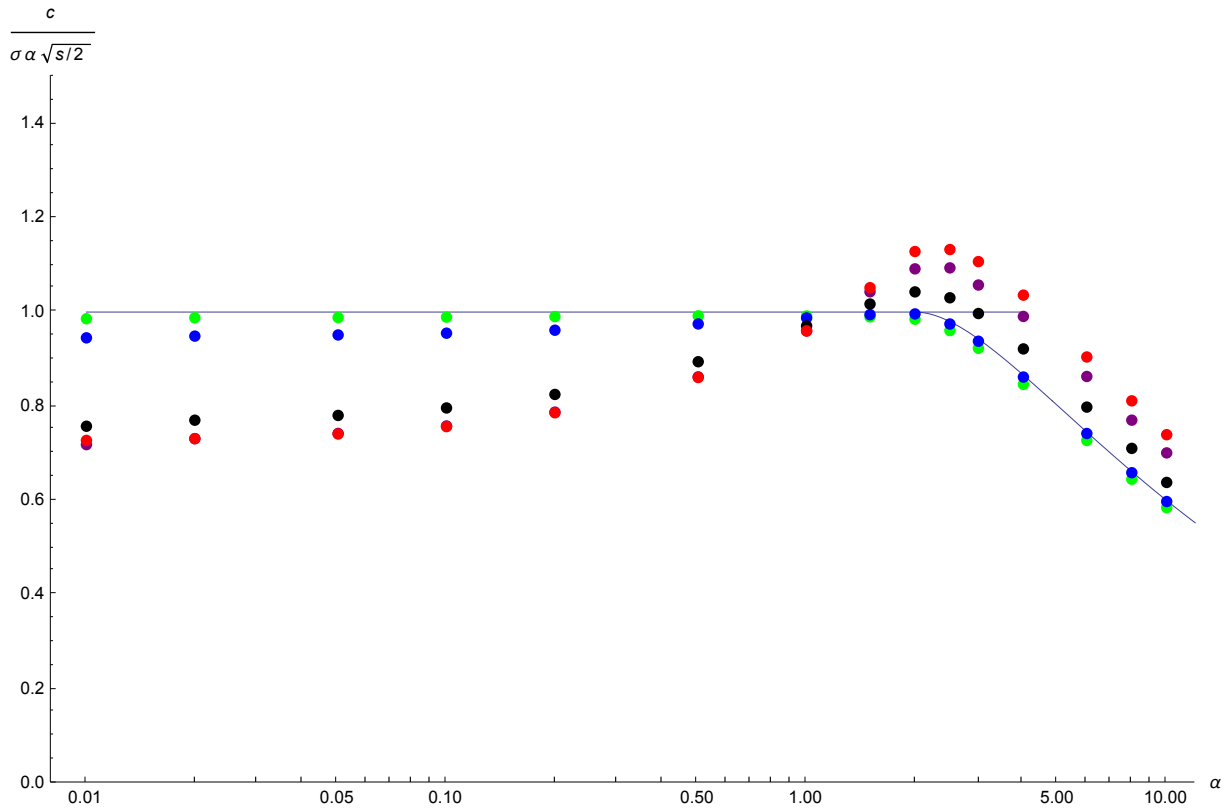


Table 1. The mass and the fraction of the total variance that is excluded by truncating distributions at 10σ (Fig. 1, green, blue, black), 25σ (Fig. 1, purple) and 50σ (Fig. 1, red).

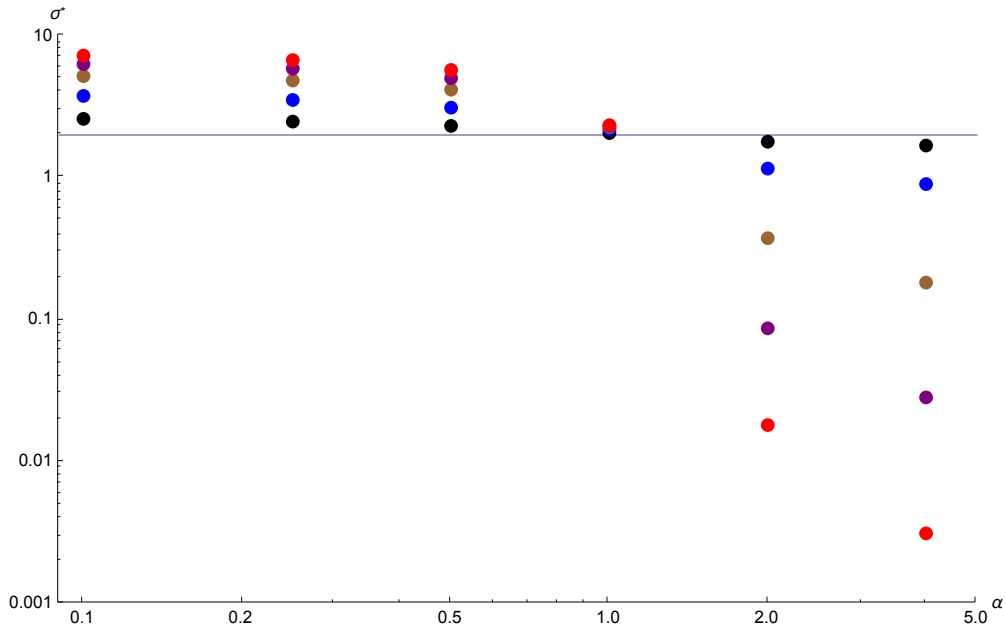
		Gaussian	Laplace	ExpSqrt
10σ	mass	1.52397×10^{-23}	7.21354×10^{-7}	0.000326548
	variance	1.55416×10^{-21}	0.0000830583	0.0513746
25σ	mass	6.11339×10^{-138}	4.41948×10^{-16}	1.14081×10^{-6}
	variance	3.83308×10^{-135}	2.92285×10^{-13}	0.000934673
50σ	mass	0.	1.95318×10^{-31}	1.67283×10^{-9}
	variance	0.	5.02302×10^{-28}	5.03447×10^{-6}

Wave speed with infinite variance

In Fig. 1, we compared dispersal distributions that were scaled to have the same variance. This approach fails for distributions such as the Cauchy, that fall away so slowly that they have infinite variance. However, we can find the Cauchy distribution that yields the same wave speed as a Gaussian with (say) $\sigma = 2$ (Fig. 3). On an infinite range, a Cauchy distribution leads to a wave with ever-increasing speed. However, the Cauchy distribution must necessarily be truncated for numerical calculations, and for any given truncation point, the wave does settle to a steady speed, which can be matched to that of a Gaussian. Figure 3 plots the standard deviation of the truncated Cauchy against $\alpha = 1 - 2\hat{p}$, for truncation at $10\sigma \dots 100\sigma$ (black ... red dots). For pushed waves ($\alpha < 2$), fat tails slow down the wave, because long-distance migrants are lost, and so the truncated Cauchy must have a higher variance to maintain the same speed ($\alpha < 2$, left of Fig. 3). For a pulled wave, however, a truncated Cauchy with a very small variance can maintain high speed, provided that it is truncated sufficiently far out. In the most extreme case shown here (truncation at 100σ , $\alpha=4$; bottom right of Fig. 3), Only a

fraction 7.9×10^{-8} disperse away from their native deme, contributing variance $\sim 10^{-5}$, and yet this maintains a wave with the same speed as Gaussian dispersal with standard deviation $\sigma=2$. (Note that for these extreme cases, the choice of deme spacing does affect the results, though not qualitatively).

Figure 2. The standard deviation, σ^* , of the truncated Cauchy distribution that gives the same speed as a Gaussian with $\sigma=2$ (horizontal line); this is plotted against α . The distribution is truncated at 10σ , 25σ , 50σ , 75σ , 100σ (black, blue, brown, purple, red).



Random fluctuations

With long-tailed dispersal, deterministic models are misleading, because the numbers of long-range migrants will be small even in very dense populations. Indeed, even with Gaussian dispersal, finite population size has an appreciable effect on the speed of a pulled wave, because the dynamics depend on regions where alleles or individuals are very rare. Here, we simulate a finite population on an infinite range. The population is represented as a list of the numbers of the focal allele in each deme; all demes to the left are assumed to be fixed, and all to the right are assumed to be at zero. In each generation, and in each deme, there is selection followed by random sampling of $2N$ genes, following the Wright-Fisher model. Dispersal is implemented as follows. For each of the n_p demes that are currently polymorphic, the $2N$ genes are drawn from a parent population according to the dispersal function; the continuous dispersal distribution is rounded to the nearest integer. (For $\sigma=2$, as used here, this causes negligible error). These genes can be from arbitrarily far away. The same procedure is followed for 1000 demes to the left of the current set, and 1000 demes to the right. Finally, the list is trimmed to remove fixed demes on the left and on the right (but tracking the location of the leftmost polymorphic deme, which will tend to move to the right as the wave advances. This scheme is extremely efficient, since the random distances moved can be taken as a single draw of $2Nn_p$ random numbers from the dispersal distribution. The only approximations are that individuals live on a discrete grid, and that only ± 1000 demes are followed on either side.

Table 2 summarises the effects of finite population size. For a pushed wave ($\alpha=0.5$), random drift has little effect, unless deme size is very small ($2N=5$). For a pulled wave, there is a substantial slowing, even for demes of $2N=1000$ individuals. Note that this stochastic effect means that long range disper-

sal no longer increases the speed of advance, even for the exponential square root. There is no sign that rare propagules move far ahead of the initial wave, producing the kind of stochastic advance that is expected for very fat-tailed distribution. The key conclusion is that random fluctuations have very little effect on the speed of “pushed” waves. The slowing effect is greater when waves are “pulled”, and there is long-range dispersal. However, even then the effect is not as dramatic as suggested by the asymptotic theory.

Table 2. The wave speed in a finite population. This is estimated as the mean speed over 2000 generations. The last row shows the results for the deterministic model (Fig. 1) with $k_{\max} = 20$ for the Gaussian and Laplace distributions, and $k_m = 200$ for the exponential square root.

$\alpha = 0.5$	$2N$	Gaussian	Laplace	ExpSqrt	$\alpha = 4$	Gaussian	Laplace	ExpSqrt
	10	0.263	0.274	0.267		0.533	0.540	0.546
	100	0.259	0.257	0.243		0.697	0.672	0.705
	1000					0.716	0.704	0.746
	∞	0.255	0.250	0.230		0.751	0.765	0.920

References not cited in the main text.

Brunet E, Derrida B, Mueller AH, Munier S (2006) Phenomenological theory giving the full statistics of the position of fluctuating pulled fronts. *Phys. Rev. E* 73: 056126.

Fisher, RA (1937) The wave of advance of advantageous genes. *Annals of Eugenics* 7: 355-369.

Stokes AN (1976) On two types of moving front in quasilinear diffusion. *Mathematical Biosciences* 31: 307-315.

Appendix B: Establishing a wave

In a bistable system, a wave can be established if the initial distribution is above some threshold. Alternatively, one might continuously release within some region: again, there will be some threshold required for establishment. If the intensity of the source is above this threshold, then the wave can be established even if the source is turned off at a finite time. A key comparison is the total number that need to be introduced to establish the wave, or (more simply) how long the source needs to continue to send out the same number as would be needed with an initial brief pulse. Our intuition is that an initial pulse would always be more efficient, since any release in regions below the threshold will decay over time: the key is to raise a sufficiently large region above the threshold so that it can contribute to further increase.

We represent an influx by a term $mf[x]q$, which represents migration from a deme fixed for $p = 1$: in each generation, a (scaled) fraction $mf(X)$ is replaced by migrants. This ensures that allele frequencies do not rise above 1. If one follows population density, scaled relative to carrying capacity, and with an Allee effect that causes bistability, then one would add a term $\lambda f[x]$, and density could rise above carrying capacity. Here we assume a source $\lambda f(X)q$, corresponding to replacement of a fraction of the population. This is appropriate if population size is regulated to a constant value after the release.

Island model

Take the simple case of a single population, with an influx that replaces a fraction m of the population every generation. Let $T = (s_h/2)t$, $M = \frac{2m}{s_h}$; $\alpha = 1 - 2\hat{p}$:

$$\frac{\partial p}{\partial T} = pq(2p - 1 + \alpha) + Mq \quad (1)$$

Then, it is easy to show that the critical migration rate is $M^* = (1 - \alpha)^2/16$. How much higher does M need to be if sustained for a finite time, T_0 ? Integrating Eq. B1, starting from zero allele frequency:

$$T = \frac{(3 + \alpha)}{\sqrt{M - M^*} (1 + M + \alpha)} \left(\text{ArcTan} \left[\frac{1 - \alpha}{\sqrt{M - M^*}} \right] - \text{ArcTan} \left[\frac{1 - 4p - \alpha}{\sqrt{M - M^*}} \right] \right) + \frac{1}{2} \left(\left(-2 \text{Log} [1 - p] + \text{Log} \left[1 + \frac{p}{M} (-1 + 2p + \alpha) \right] \right) \right) / (1 + M + \alpha) \quad M^* = \frac{(1 - \alpha)^2}{8} \quad (2)$$

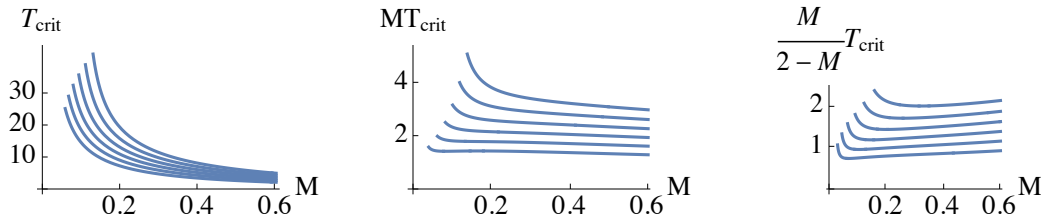
Now, establishment is assured if, at time T_{crit} , $p > \hat{p} = \frac{(1-\alpha)}{2}$. Setting $p = \frac{(1-\alpha)}{2}$:

$$T_{\text{crit}} = \frac{2(3 + \alpha)}{\sqrt{M - M^*} (1 + M + \alpha)} \text{ArcTan} \left[\frac{(1 - \alpha)}{\sqrt{M - M^*}} \right] - \frac{\text{Log} \left[\frac{1 + \alpha}{2} \right]}{(1 + M + \alpha)} \quad (3)$$

The left plot of Fig. B1 shows this critical time, as a function of the scaled migration rate, M . One might measure the total 'cost' of the introduction by MT . This declines to an asymptote for large M , indicating that the most efficient strategy is a short pulse that quickly raises the frequency above the critical threshold. However, MT is almost constant above $M \sim 0.1$, and so the precise timing of the introduction makes little difference (Fig. B1, middle). If the resident population is constant, N_0 , then the number that need to be introduced to replace a fraction m is $\frac{m}{1-m} N_0$. With complete CI, $s_h = 1$, and so, this equals $\frac{M}{2-M}$: it becomes expensive to replace a large fraction of the population. When this effect is

included (Fig. B1, right), the most efficient strategy is at intermediate M . However, an instantaneous pulse is almost as efficient. The best guidance is that the introduction should be made as rapidly as is feasible, given practical constraints.

Figure B1: The left plot shows the minimum time needed for establishment, plotted against $M = \frac{2m}{s_h}$, as a function of $\alpha = 0.1, 0.2, 0.3, 0.4, 0.5, 0.6$ (bottom to top) (i.e., $\hat{p} = 0.45, 0.4, 0.35, 0.3, 0.25, 0.2$). The middle plot shows $MT_{\text{crit}} = m t_{\text{crit}}$, and the right plot $\frac{M}{2-M} T_{\text{crit}} = \frac{m}{2(1-m/s_h)} t_{\text{crit}}$



One dimension

We rescale Eqs. 2, 3 by setting time to $T = (s_h/2) t$ and distance to $X = x \sqrt{s_h} / \sigma$; $M = \frac{2m}{s_h}$, $\alpha = 1 - 2\hat{p}$:

$$\frac{\partial p}{\partial T} = \frac{\partial^2 p}{\partial X^2} + pq(2p - 1 + \alpha) + M[X]q \quad (4)$$

With $M=0$, the wave will increase if the initial $p[X, 0]$ is “large enough”. There is a critical bubble that lies on this threshold, which can be calculated explicitly in one dimension. Now, suppose that initially $p=0$. How large must M be to ensure spread? This can be solved for special choices of the source, $M[X]$; below, we give the critical value for a point source, and for a “top hat” function, with a constant input within some region. We then give numerical results for the minimum time needed to ensure establishment, analogous to Fig. B1.

Point source

With a source $M\delta(X)q$, there is a boundary condition $p'[0, T] = \pm Mq[0, T]/2$. Integrating Eq. 1 we have, at $X=0$:

$$\frac{\partial p}{\partial X} = p \sqrt{q^2 - \alpha \left(1 - \frac{2}{3} p\right)} = \frac{M}{2} q \quad (5)$$

The function $2 \frac{p}{q} \sqrt{q^2 - \alpha \left(1 - \frac{2}{3} p\right)}$ has an intermediate maximum, which gives the threshold value of Λ . Below this threshold, there are two solutions for p , one stable and one unstable:

$$M_{\text{crit}} = B \sqrt{1 - 4\alpha \frac{(1 - B/3)}{(2 - B)^2}}$$

$$\text{where } B = 2 \left(1 - \frac{\alpha}{9}\right) - 2\alpha \left(1 + \frac{\alpha}{9}\right) \left(\frac{\Lambda}{2}\right)^{-1/3} - \frac{(4\Lambda)^{1/3}}{9}, \quad (6)$$

$$A = 243 \alpha \left(1 + \frac{\alpha}{9} + \frac{2 \alpha^2}{243} - \sqrt{1 + \frac{14}{81} \alpha + \frac{\alpha^2}{81}} \right)$$

In the original variables, the threshold scales as $\Lambda > g[\alpha] \frac{\sigma}{2} \sqrt{s_h}$ which has the dimensions XT^{-1} .

Top-hat source

Now, suppose that we have a source Mq within $-Y < X < Y$. Then, equilibrium is given by:

$$\begin{aligned} 0 &= \frac{\partial^2 p}{\partial X^2} + p(1-p)(2p-1+\alpha) + Mq & (0 < X < Y) \\ 0 &= \frac{\partial^2 p}{\partial X^2} + p(1-p)(2p-1+\alpha) & (Y < X) \end{aligned} \quad (7)$$

with $p'[0] = 0$, $p[Y_-] = p[Y_+]$, $p'[Y_-] = p'[Y_+]$

Integrating:

$$\begin{aligned} \left(\frac{\partial p}{\partial X} \right)^2 &= h[p] \quad (Y < X) \\ \left(\frac{\partial p}{\partial X} \right)^2 &= h[p] - M(p - p_Y)(2 - p_Y - p) \quad (0 < X < Y) \end{aligned} \quad (8)$$

$$\text{where } h[p] = p^2 \left((1-p)^2 - \alpha \left(1 - \frac{2}{3} p \right) \right)$$

The allele frequency at zero, p_0 , is where $\partial p / \partial X = 0$, so that $0 = h[p_0] - M(p_0 - p_Y)(2 - p_0 - p_Y)$; this defines p_0 as a function of p_Y . We can obtain Y by integrating $\partial X / \partial p$. Hence, p_Y is given by:

$$Y = \int_{p_Y}^{p_0} \frac{dp}{\sqrt{h[p] - M(p - p_Y)(2 - p_0 - p_Y)}} \quad (9)$$

For given p_Y , there is a solution for Y , provided that $p_Y < \frac{2}{3}$; this has a maximum value of Y_{crit} , so that if $Y < Y_{\text{crit}}$, there will be two solutions. This maximum defines the threshold for spread. However, it is not straightforward to find this threshold analytically.

Consider the equation $0 = h[p_0] - M(p_0 - p_Y)(2 - p_0 - p_Y)$. For $M > (1 - \alpha)^2 / 8$, there is only one root. For $M < (1 - \alpha)^2 / 8$, there is one root if $p_Y > p_Y^*$.

$$\begin{aligned} p_0^* &= \frac{1}{4} (1 - \alpha - \sqrt{A}) \\ p_Y^* &= 1 - \frac{1}{4 \sqrt{6M}} \sqrt{((1 - \alpha)^3 (3 + \alpha) + 12(5 + 2\alpha + \alpha^2)M - 24M^2 - A \sqrt{A} (3 + \alpha))} \end{aligned} \quad (10)$$

$$\text{where } A = (1 - \alpha)^2 - 8M.$$

For $M > (1 - \alpha)^2 / 8 = 0.02$, there is a single solution, with a peak which represents the maximum Y_{crit} consistent with a stable equilibrium. However, once M passes below the threshold, there is a singularity, and it appears that there can be a stable solution with extremely large Y . This threshold simply corresponds to M so low that it cannot cause a transition, even as $Y \rightarrow \infty$. Fig. B2 shows solutions to Eq. 10 over a range of α, \hat{p} ; the maximum gives the critical spatial range, Y_{crit} , required for establishment. Table B1 gives this maximum, together with the total input, $2MY_{\text{crit}}$. For given α, \hat{p} , there is an optimal migration rate and spatial extent that minimises $2MY_{\text{crit}}$. These analytic results give the minimum input required for establishment. However, it would take an indefinitely long time for establish-

ment to be assured. If the input is more intense and/or over a wider spatial range, then it could persist for a shorter time. Results for a finite time, analogous to the island model (Fig. B1), require numerical solution. We give those in the next section, for two dimensions.

Figure B2. The value of Y against p_Y , for $\alpha=0.2$, $\hat{p}=0.2$, and $M= 0.02, 0.03, 0.04, 0.05, 0.06$ (top to bottom). The maximum Y corresponds to the minimum size of the range, $\{-Y, Y\}$ necessary for establishment, given a source M .

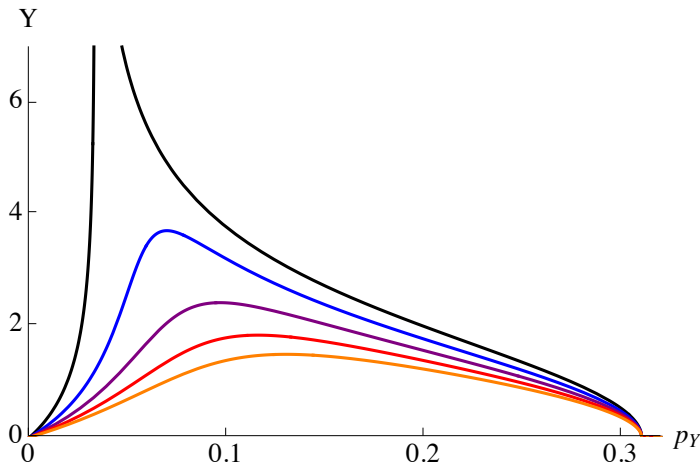


Table B1. Threshold Y_{crit} for varying α , M . p_Y , p_0 give the frequency at the edge of the source and at the centre, respectively. $2MY_{crit}$ gives the total rate of input. The last column, M_δ , gives the critical intensity of point source needed to allow establishment; it is the limit of the the total source $2MY$ when M becomes large and its spatial extent, $\{-Y, Y\}$ small.

α	\hat{p}	M	p_Y	p_0	Y_{crit}	$2MY_{crit}$	M_δ
0.1	0.45	0.10			∞	∞	
		0.15	0.156	0.339074	2.86202	0.858606	
		0.2	0.230	0.397044	1.93251	0.773003	
		0.3	0.339	0.470151	1.2619	0.757142	
		0.4	0.408	0.512299	0.964945	0.771956	
		0.5	0.452	0.537759	0.789265	0.789265	
		0.6	0.483	0.554738	0.670762	0.804915	
		0.7	0.504	0.566513	0.584561	0.818385	0.956562
0.2	0.4	0.08			∞	∞	
		0.1	0.104	0.266342	4.13891	0.827782	
		0.15	0.189	0.333694	2.10228	0.630685	
		0.2	0.251	0.373722	1.50629	0.602516	
		0.3	0.328	0.418784	0.999828	0.599897	
		0.4	0.372	0.44259	0.760042	0.608034	0.684528
0.4	0.3	0.045			∞	∞	
		0.05	0.062	0.180264	6.71364	0.671364	
		0.1	0.163	0.25412	1.83648	0.367296	
		0.15	0.215	0.28246	1.17168	0.351503	
		0.2	0.245	0.297788	0.87301	0.349204	
		0.3	0.278	0.313796	0.584271	0.350562	
		0.4	0.295	0.322091	0.440908	0.352726	0.366544
0.6	0.2	0.02	0.033	0.100	∞		

0.05	0.116	0.168	1.83167	0.183167	
0.1	0.162	0.191	0.866468	0.173294	
0.15	0.179	0.199	0.575105	0.172531	
0.2	0.189	0.203	0.431589	0.172635	
0.3	0.198	0.208	0.288481	0.173089	
0.4	0.203	0.210	0.21682	0.173456	0.175184

Two dimensions

Using the same scalings as in one dimensions, we have:

$$\frac{\partial p}{\partial T} = \frac{\partial^2 p}{\partial R^2} + \frac{1}{R} \frac{\partial p}{\partial R} + pq(2p - 1 + \alpha) + M[R]q \quad (11)$$

We solve this equation numerically using `NDSolve` in *Mathematica*. For a given α, \hat{p} , there is a critical radius, R_{crit} , such that the wave will just establish if initially $p = 1$ within $R < R_{\text{crit}}$. We compare this initial pulse with a continuous source within the same radius, and sustained for time T ; for given T , we find the minimum M required for establishment; this also gives the minimum T_{crit} needed for establishment with given M . As M increases above the threshold required for establishment from an indefinitely sustained source, T_{crit} decreases. Figure B3 summarises these results, in the same form as for Fig. B1, but just for $\alpha = 0.6, \hat{p} = 0.2$. As for the island model, the effort, measured by MT reaches an asymptote for large M , indicating that an immediate increase to high frequency is most efficient. If the increasing cost of raising frequency by introduction into a fixed native population is included, by using the measure $\frac{M}{2-M} T_{\text{crit}}$, then the most efficient scheme is to use $M \sim 0.3$ for $T_{\text{crit}} \sim 1$ - which is still an extremely short time if $s_h = 1$.

Figure B3. On the left, the time for which a source needs to be sustained, plotted against source strength, M , given optimal initial radius. The vertical line is the source strength needed for establishment, if sustained indefinitely. The middle plot shows the total amount, $MT_{\text{crit}} = \frac{m}{2} t_{\text{crit}}$ that is needed, as a function of source strength. The right plot shows $\frac{M}{2-M} T_{\text{crit}} = \frac{m}{2(1-m/s_h)} t_{\text{crit}}$, which is the total number that need to be introduced, relative to a constant native population, if $s_h = 1$. $R_{\text{crit}} = 5.19, \alpha = 0.6, \hat{p} = 0.2$.

